



HAL
open science

CC17 group B Streptococcus exploits integrins for neonatal meningitis development

Romain Deshayes de Cambronne, Agnès Fouet, Amandine Picart, Anne-Sophie Bourrel, Cyril Anjou, Guillaume Bouvier, Cristina Candeias, Abdelouhab Bouaboud, Lionel Costa, Anne-Cécile Boulay, et al.

► To cite this version:

Romain Deshayes de Cambronne, Agnès Fouet, Amandine Picart, Anne-Sophie Bourrel, Cyril Anjou, et al.. CC17 group B Streptococcus exploits integrins for neonatal meningitis development. The Journal of clinical investigation, 2021, 131 (5), pp.e136737. 10.1172/JCI136737 . hal-03408728v2

HAL Id: hal-03408728

<https://hal.science/hal-03408728v2>

Submitted on 2 Nov 2021

HAL is a multi-disciplinary open access archive for the deposit and dissemination of scientific research documents, whether they are published or not. The documents may come from teaching and research institutions in France or abroad, or from public or private research centers.

L'archive ouverte pluridisciplinaire **HAL**, est destinée au dépôt et à la diffusion de documents scientifiques de niveau recherche, publiés ou non, émanant des établissements d'enseignement et de recherche français ou étrangers, des laboratoires publics ou privés.



Distributed under a Creative Commons Attribution - NonCommercial 4.0 International License

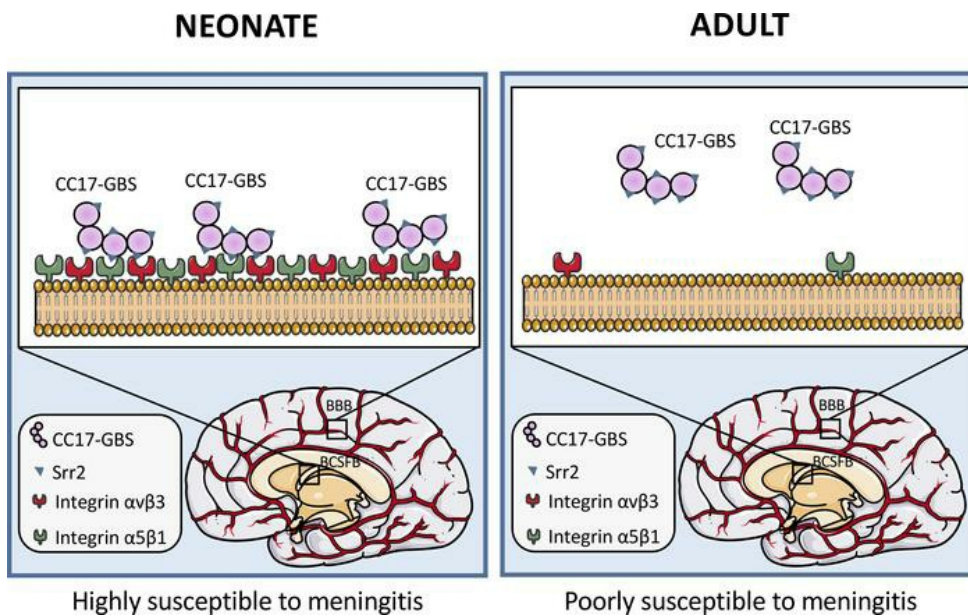
CC17 Group B *Streptococcus* exploits integrins for neonatal meningitis development

Romain Deshayes de Cambronne, ... , Claire Poyart, Julie Guignot

J Clin Invest. 2021. <https://doi.org/10.1172/JCI136737>.

Research In-Press Preview Infectious disease Microbiology

Graphical abstract



Find the latest version:

<https://jci.me/136737/pdf>



1 **CC17 Group B *Streptococcus* exploits integrins for neonatal meningitis development**

2

3 Romain Deshayes de Cambrone¹, Agnès Fouet¹, Amandine Picart¹, Anne-Sophie Bourrel^{1,2},
4 Cyril Anjou¹, Guillaume Bouvier⁴, Cristina Candeias¹, Abdelouhab Bouaboud¹, Lionel Costa¹,
5 Anne-Cécile Boulay⁵, Martine Cohen-Salmon⁵, Isabelle Plu⁶, Caroline Rambaud⁷, Eva
6 Faurobert⁸, Corinne Albigès-Rizo⁸, Asmaa Tazi^{1,2,3}, Claire Poyart^{1,2,3}, Julie Guignot^{1*}

7

8 ¹Université de Paris, Institut Cochin, INSERM, U1016, CNRS, UMR8104, F-75014 Paris,
9 France; ²Hôpitaux Universitaires Paris Centre, Cochin, Assistance Publique Hôpitaux de Paris,
10 France; ³Centre National de Référence des Streptocoques, France; ⁴Structural Bioinformatics
11 Unit, Department of Structural Biology and Chemistry, Institut Pasteur, CNRS UMR3528, C3BI,
12 USR3756 Paris, France; ⁵Center for Interdisciplinary Research in Biology (CIRB), Collège de
13 France, CNRS UMR7241, INSERM U1050, PSL Research University, Paris, France;
14 ⁶Sorbonne Université /Département de neuropathologie Raymond Escourolle - Hôpital Pitié-
15 Salpêtrière - Assistance Publique-Hôpitaux de Paris, France; ⁷Université de Versailles Saint
16 Quentin en Yvelines (Université Paris-Saclay)/Service d'anatomie-pathologique et médecine
17 légale, Hôpital Raymond Poincaré, Garches, France; ⁸INSERM U1209, CNRS UMR 5309,
18 Institute for Advanced Biosciences, France/Université Grenoble Alpes, F-38700 La Tronche,
19 France.

20 * To whom correspondence should be addressed: julie.guignot@inserm.fr

21 ORCID number: [0000-0001-8890-4028](https://orcid.org/0000-0001-8890-4028). Tel: + 33 1 40 51 64 13; Fax: + 33 1 40 51 64 54.

22 Institut Cochin, 22 rue Méchain 75014 Paris, France.

23 **CONFLICT OF INTEREST:**

24 The authors have declared that no conflict of interest exists.

25 **KEYWORDS:** Srr2, CC17, *Streptococcus agalactiae*, Group B Streptococcus, meningitis,
26 integrin, neonatal susceptibility, blood brain barrier (BBB)

27

28 **ABSTRACT**

29 Group B *Streptococcus* (GBS) is the major cause of human neonatal infections. A single clone,
30 designated CC17-GBS, accounts for more than 80% of meningitis cases, the most severe form of
31 the infection. However, the events allowing blood-borne GBS to penetrate the brain remain largely
32 elusive. In this study, we identified the host transmembrane receptors $\alpha 5\beta 1$ and $\alpha v\beta 3$ integrins as
33 the ligands of Srr2, a major CC17-GBS specific adhesin. Two motifs located in the binding region
34 of Srr2 were responsible for the interaction between CC17-GBS and these integrins. We
35 demonstrated, in a blood-brain barrier cellular model, that both integrins contributed to the
36 adhesion and internalization of CC17-GBS. Strikingly, both integrins were overexpressed during
37 the post-natal period in the brain vessels of the blood-brain and blood-cerebrospinal fluid barriers
38 and contributed to the juvenile susceptibility to CC17-meningitis. Finally, blocking these integrins
39 decreased CC17-GBS crossing into the juvenile mice central nervous system in an *in vivo* model
40 of meningitis.

41 Our study demonstrates that CC17-GBS exploits integrins for crossing the brain vessels leading
42 to meningitis. Importantly, it provides host molecular insights into neonate's susceptibility to CC17-
43 GBS meningitis, thereby opening new perspectives for therapeutic and prevention strategies of
44 GBS-elicited meningitis.

45

46 INTRODUCTION

47 In the early 1950's, due to the massive utilization of tetracyclines, *Streptococcus agalactiae* (Group
48 B *Streptococcus*, GBS) emerged worldwide as the most significant pathogen causing severe
49 neonatal invasive infections (1). This commensal bacterium, which is found in the intestine and
50 the genital tract of 11 to 22% of healthy humans (2), is responsible for two syndromes in neonates,
51 the early-onset disease (EOD) which occurs within the first 48 hours after birth in 90% of the cases,
52 and the late-onset disease (LOD) which occurs between 7 and 89 days of life (3). EOD results
53 from mother-to-child vertical transmission of the bacterium through the inhalation of GBS-
54 contaminated amniotic fluid or vaginal secretions during delivery. EOD often manifests by
55 bloodstream infections that are complicated by meningitis in 15 to 30% of the cases (4). The onset
56 of LOD remains largely unknown, although recent studies argue for the co-existence of both
57 *intrapartum* and post-natal transmission routes and for a gastrointestinal portal of entry (5-7).
58 Meningitis is common during LOD, up to 50% of the cases, mainly due to one particular GBS clone
59 almost exclusively of capsular serotype III and belonging to the clonal complex (CC) 17. Overall,
60 as reported by worldwide epidemiological studies, the so-called hypervirulent CC17-GBS is
61 responsible for 80% to 95% of the cases of neonatal GBS-elicited meningitis, both syndromes
62 combined, highlighting a strong meningeal tropism (4, 8-11).

63 The critical step for meningitis development is the transmigration of blood-borne-GBS into the
64 central nervous system (CNS). Brain is normally protected by physiological barriers that separate
65 the blood from the brain parenchyma or the cerebrospinal fluid. Brain microvascular endothelial
66 cells and choroid plexus epithelial cells that compose the blood-brain barrier (BBB) and the blood-
67 cerebrospinal fluid barrier (BCSFB), respectively, are both characterized by the presence of tight
68 junctions that are crucial for the maintenance of the barrier function. To penetrate those barriers,
69 blood-borne bacteria can either use a transcellular mechanism that requires pathogen
70 internalization and/or a paracellular mechanism that requires tight junction disruption. Alternatively
71 bacteria can use phagocytes as Trojan horse (12). GBS has been described to be internalized in

72 cerebral endothelial cells, but also to inhibit tight junction proteins expression, suggesting that
73 GBS could use trans and/or paracellular mechanisms to penetrate the brain (13, 14).
74 CC17 strains were shown to display higher adherence properties to brain endothelial cells
75 compared to non-CC17 strains (15). Two CC17-GBS specific surface adhesins, Srr2 and HvgA,
76 account for the increased binding of CC17-GBS to brain endothelial cells compared to non-CC17
77 strains and contribute to BBB crossing in *in vivo* model of meningitis (15, 16). However, how these
78 proteins contribute to brain barrier crossing at the molecular level is currently unknown.
79 Here, we demonstrate that Srr2 directly and specifically binds to integrins $\alpha 5\beta 1$ and $\alpha v\beta 3$, thereby
80 contributing to the adhesion and invasion of brain endothelial cells and to the crossing of brain
81 barriers leading to meningitis development.
82 Most importantly, we show that these receptors are overexpressed during the postnatal period in
83 brain vessels, arguing for CC17-GBS increased invasiveness of the CNS in neonates.

84

85 RESULTS

86 ***The Binding Region (BR_{Srr2}) of the Srr2-CC17 specific adhesin interacts with $\alpha5\beta1$ and $\alpha\nu\beta3$*** 87 ***integrins***

88 In contrast to HvgA for which no molecular ligand has been identified, Srr2 contains a fibrinogen-
89 binding site within the region, termed Binding Region (BR_{Srr2}), involved in CC17-GBS adhesion to
90 a variety of host cells (16-19). A Srr2-homologous protein, designated Srr1, which also possesses
91 a fibrinogen binding site in its Binding Region (BR_{Srr1}), is expressed by non-CC17 GBS isolates.
92 Although Srr2 and Srr1 have a similar structure, they display only 37% amino–acid sequence
93 identity in their Binding Regions (Fig.1A). Looking in BR_{Srr2} for binding motifs which could account
94 for the hyper-adhesion phenotype properties of CC17-GBS to host cell, we identified by sequence
95 analysis an Arg-Gly-Asp (RGD) and a Ser-Asp-Val (SDV) motifs which are absent from BR_{Srr1}
96 (Fig.1A). These two motifs are known to allow integrin recognition (20, 21). Integrins are
97 transmembrane heterodimeric receptors composed of one α and one β subunit that combine to
98 form up to 24 different integrins. While the SDV motif has been recently identified to be specific of
99 $\alpha\nu\beta3$, the RGD motif is recognized by a number of different integrins (22, 23). We therefore
100 focused our study on $\alpha5\beta1$ and $\alpha\nu\beta3$ integrins known to recognize RGD or SDV motifs and, to be
101 expressed by brain endothelial cells as CC17 strains are highly correlated to meningitis (24, 25).

102 We therefore compared the interaction of BR_{Srr2} and BR_{Srr1} with $\alpha5\beta1$ and $\alpha\nu\beta3$ integrins. We first
103 measured by immunoblotting the direct binding of BR_{Srr2} and BR_{Srr1} to immobilized recombinant
104 soluble human integrins $\alpha5\beta1$ and $\alpha\nu\beta3$. Intense signals were obtained with BR_{Srr2} where $\alpha5\beta1$
105 and $\alpha\nu\beta3$ integrins were spotted, but not where ICAM1, another transmembrane protein, was
106 spotted, indicating that BR_{Srr2} binds to recombinant human $\alpha5\beta1$ and $\alpha\nu\beta3$ integrins (Fig. 1B). In
107 contrast, weak signals were observed when BR_{Srr1} was assayed in the same conditions with $\alpha5\beta1$
108 and $\alpha\nu\beta3$ integrins (Fig. 1B).

109 The interaction between BR_{Srr2} and human $\alpha 5\beta 1$ and $\alpha v\beta 3$ integrins was further confirmed by
110 ELISA assays showing that recombinant human $\alpha 5\beta 1$ and $\alpha v\beta 3$ integrins bind to immobilized
111 BR_{Srr2} in a saturable and dose-dependent manner, whereas they failed to bind to BR_{Srr1} (Fig. 1C
112 and 1D). As a control, ICAM1 bound neither to BR_{Srr2} nor to BR_{Srr1} (Fig. 1E). Moreover, no
113 interaction was observed between the $\alpha 5\beta 1$ and $\alpha v\beta 3$ integrins and HvgA, the other CC17-GBS
114 specific adhesin (data not shown).

115 Integrin structure and ligand binding affinity are strongly affected by divalent cations
116 concentrations (26). This property was confirmed for BR_{Srr2}-integrin interaction by ELISA assays
117 in presence of CaCl₂ or MnCl₂. Addition of Ca²⁺ or Mn²⁺ totally abolished $\alpha 5\beta 1$ integrin binding to
118 BR_{Srr2}, while Ca²⁺ strongly enhanced $\alpha v\beta 3$ integrin binding to BR_{Srr2} (Fig. S2A and B). Last, the
119 interaction between BR_{Srr1} and BR_{Srr2} with non-RGD recognizing integrins expressed by brain
120 endothelial cells ($\alpha 6\beta 1$; $\alpha 4\beta 1$; $\alpha 3\beta 1$) and non-RGD recognizing integrins described to directly bind
121 to GBS ($\alpha 1\beta 1$) were analyzed (24, 27). Interestingly, both BR_{Srr1} and BR_{Srr2} interacted with $\alpha 6\beta 1$;
122 $\alpha 4\beta 1$; $\alpha 3\beta 1$ integrins, however this is not a general feature to all integrins as $\alpha 1\beta 1$ failed to bind
123 both BR_{Srr1} and BR_{Srr2} (Fig. S3).

124 Altogether, our data show that $\alpha 5\beta 1$ or $\alpha v\beta 3$ integrins are directly and specifically recognized by
125 BR_{Srr2}.

126

127 ***$\alpha v\beta 3$ -BR_{Srr2} interaction depends on the RGD and SDV motifs***

128 In order to test the role of the RGD and SDV motifs present on BR_{Srr2} in their interaction with
129 integrins, mutated forms of BR_{Srr2} were produced in which the RGD or/and the SDV motifs were
130 replaced by three alanines (Fig. S1B and C). The interaction between BR_{Srr2} mutated forms with
131 integrins $\alpha v\beta 3$ or $\alpha 5\beta 1$ was assessed by ELISA. RGD and/or SDV substitutions strongly affected

132 $\alpha v\beta 3$ integrin binding (Fig. 2A), but not that with $\alpha 5\beta 1$ integrin (Fig. 2B). No additive inhibition was
133 observed when both motifs (RGD and SDV) were mutated (Fig. 2A).

134 The contribution of these motifs to integrin binding was further supported by competitive ELISA
135 assays using synthetic peptides containing an RGD sequence (RGDS and RGDfV peptides) or
136 an SDV sequence (P11 peptide) that are widely used to inhibit integrin recognition (20, 21). RGD
137 and SDV peptides significantly inhibited $\alpha v\beta 3$ -BR_{Srr2} interaction in a dose-dependent manner,
138 whereas they had no significant effect on $\alpha 5\beta 1$ - BR_{Srr2} interaction (Fig. 2C and 2D).

139 Altogether, these results demonstrate that the interaction of BR_{Srr2} with integrin $\alpha v\beta 3$ requires both
140 RGD and SDV motifs, whereas the interaction with integrin $\alpha 5\beta 1$ is independent from these motifs.

141

142 ***BR_{Srr2} interaction with integrin $\alpha 5\beta 1$ involves two other motifs***

143 To identify BR_{Srr2} residues involved in $\alpha 5\beta 1$ integrin recognition, we used the RaptorX webserver
144 which enables, by combining co-evolution and deep learning, to predict residue - residue
145 interactions (28). Using this approach, two putative motifs of interaction between BR_{Srr2} and $\alpha 5\beta 1$
146 were identified (Fig. S4A and Fig. 2E). The first one is an FSVKI motif located in the N-terminal
147 subdomain of BR_{Srr2} at position 362 and the second one is an ETYVI motif located in the C-terminal
148 subdomain of BR_{Srr2} at position 496 (Fig. 2E and 2F). These two motifs are absent from the BR_{Srr1}
149 sequence. To address the role of these two motifs in the interaction with integrin $\alpha 5\beta 1$, we first
150 addressed the binding capacities of BR_{Srr2} subdomains containing these motifs. The N-terminal
151 and C-terminal subdomains of BR_{Srr2} containing either motif were produced, and equimolar amount
152 of full length BR_{Srr2}, N-terminal and C-terminal domains were used to perform ELISA binding
153 assays. The $\alpha 5\beta 1$ integrin displayed a similar capacity to bind to all three forms of BR_{Srr2} (Fig. 2G)
154 indicating the presence of at least one binding motif on each of BR_{Srr2} sub-domains.

155 We next generated mutated forms of BR_{Srr2} in which the FSVKI or the ETYVI sequences were
156 replaced by FAAAI and AAYAI, respectively (Fig. S1D and E) and the interaction with integrin

157 $\alpha 5\beta 1$ was assessed by ELISA. While the mutation of the ETYVI motif affects the interaction with
158 $\alpha 5\beta 1$ integrin only at the highest concentration, the mutation of the FSVKI motif significantly
159 reduced the binding to $\alpha 5\beta 1$ integrin at most concentrations (Fig. 2H).

160 Altogether, we identified the FSVKI motif of BR_{Srr2} as required for $\alpha 5\beta 1$ integrin recognition.
161 Besides, we demonstrated that BR_{Srr2} contains at least one other integrin $\alpha 5\beta 1$ recognition motif
162 which is located in its C-terminal region but remains to be identified. Interestingly, when integrin
163 binding motifs were highlighted on BR_{Srr2}, we noticed that both $\alpha v\beta 3$ binding motifs (RGD and
164 SDV) are localized on the same side of BR_{Srr2}, while $\alpha 5\beta 1$ binding motif, FSVKI, is located on the
165 opposite side (Fig. S4B).

166
167 ***Human $\alpha 5\beta 1$ integrin acts as a receptor for Srr2-expressing GBS in a simplified model of***
168 ***CHO cells***

169 To determine whether $\alpha 5\beta 1$ and $\alpha v\beta 3$ integrins are viable candidate-receptors for adhesion and/or
170 invasion of CC17-GBS, the binding of a CC17-GBS strain to a simplified model where cells
171 ectopically express human $\alpha 5\beta 1$ or $\alpha v\beta 3$ integrins was assessed. We infected the Chinese
172 Hamster Ovary (CHO) control cell line, which does not express endogenous $\beta 3$ nor $\alpha 5$ integrin
173 subunits and which is therefore deficient for the expression of $\alpha 5\beta 1$ and $\alpha v\beta 3$ integrins (29), or
174 CHO cells stably transfected with plasmids encoding human $\alpha 5\beta 1$ (CHO- $\alpha 5\beta 1$), human $\alpha v\beta 3$
175 (CHO- $\alpha v\beta 3$) or human ICAM1 as a control (30-32).

176 Numerous CC17-GBS were observed adhering to CHO- $\alpha 5\beta 1$ cells (Fig. 3A arrows) as compared
177 to non-transfected CHO or CHO-ICAM1 cells that were non-permissive for CC17 adhesion where
178 most streptococci were found unbound to cells (Fig. 3 A, arrow heads). Immunostaining with anti-
179 $\alpha 5$ antibody showed that CC17-GBS were almost exclusively associated to cells expressing
180 integrin $\alpha 5\beta 1$, while very rare bacteria were associated with cells that had lost its expression (Fig.

181 3B). In addition, few CC17-GBS bacteria adhered to CHO- $\alpha v\beta 3$ (Fig. 3A). However, only the
182 adhesion to $\alpha 5\beta 1$ expressing cells was statistically significant (Fig. 3C). We next analyzed the
183 specificity of CC17-GBS interaction with $\alpha 5\beta 1$ integrin by testing adhesion of a non-CC17 GBS
184 strain (CC23) expressing the Srr1 surface protein to CHO transfected cells. The CC23 GBS strain
185 did not show proficient adhesion to any CHO cell lines tested (Fig. 3C). Altogether, these results
186 indicate that integrin $\alpha 5\beta 1$ is an effective and specific host receptor for CC17-GBS.

187 To demonstrate that the binding to $\alpha 5\beta 1$ integrin by CC17-GBS was dependent on Srr2, we tested
188 the adhesion of CC17 $\Delta srr2$ derived strains. The adhesion of the $\Delta srr2$ mutant strain to CHO- $\alpha 5\beta 1$
189 revealed a clear defect when compared to that of the isogenic wild type (WT) strain.
190 Complementation of the $\Delta srr2$ mutant with a plasmid expressing BR_{Srr2} domain was sufficient to
191 restore adhesion to WT level. In agreement with this result, adhesion of CC17-GBS to CHO- $\alpha 5\beta 1$
192 was inhibited by anti-Srr2 antibody. Altogether, these data demonstrate that Srr2 is responsible
193 for CC17-GBS adhesion to $\alpha 5\beta 1$ integrin (Fig. 3D).

194 Finally, using a differential staining allowing to discriminate extracellular from intracellular
195 streptococci, we were able to detect internalized CC17-GFP bacteria in CHO- $\alpha 5\beta 1$ cells (Fig. 3E).
196 Comparing invasion rates obtained with CHO- $\alpha 5\beta 1$ and with untransfected cells, by CFU counting,
197 indicated that $\alpha 5\beta 1$ integrin also promotes CC17-GBS internalization in a Srr2-dependant manner
198 (Fig. 3F).

199 In conclusion, our data demonstrate that Srr2 expression allows $\alpha 5\beta 1$ integrin recognition
200 promoting CC17-GBS adhesion and invasion in a simplified cellular model.

201
202 ***$\alpha 5\beta 1$ and $\alpha v\beta 3$ integrins promote the binding and invasion of CC17-GBS to cerebral***
203 ***endothelial cells***

204 Blood-borne CC17-GBS must interact with the luminal face of cerebral endothelial cells to access
205 CNS. Because integrins are known to be expressed on the luminal and abluminal faces of

206 endothelial cells (33-36), we addressed the role of integrins in a more physiological relevant model
207 of cerebral endothelial cells. We previously showed that CC17-GBS display a hyper-adhesion
208 phenotype on cerebral endothelial cells compared to non-CC17 GBS strains (15). Both CC17
209 specific adhesins HvgA and Srr2 contribute to the adhesion properties of CC17-GBS (15, 17).
210 Therefore, we proposed to address the role of Srr2-integrin interaction in CC17-GBS adhesion to
211 cells of the BBB. We first confirmed, using the human cerebral endothelial cell line hCMEC/D3,
212 that CC17-GBS adheres, in a Srr2-dependent manner, more than the non-CC17 strain (CC23)
213 (Fig. 4A). Since the expression of bacteria recognizing cellular receptors may change upon
214 infection, we analyzed integrins expression. Expression of $\alpha 5\beta 1$ and $\alpha v\beta 3$ were not modified by
215 infection with CC17-GBS for up to 3 hours neither at the transcriptional level (Fig. S5A and C) nor
216 at the protein level (Fig. S5B and D). To investigate if $\alpha 5\beta 1$ and $\alpha v\beta 3$ integrins could contribute to
217 CC17 hyper-adhesion to brain endothelial cells, we performed competition experiments with
218 soluble integrins. When CC17-GBS were pre-incubated with soluble human $\alpha 5\beta 1$ or $\alpha v\beta 3$
219 integrins, CC17 adhesion to hCMEC/D3 was significantly reduced compared to that of the
220 untreated control (Fig. 4B). No additive effect was observed when both $\alpha 5\beta 1$ and $\alpha v\beta 3$ integrins
221 were mixed. As a control, pre-incubation with soluble ICAM1 did not alter CC17-GBS adhesion.
222 Neither $\alpha 5\beta 1$, nor $\alpha v\beta 3$ integrins, nor ICAM1 soluble protein affected the adhesion of the $\Delta srr2$
223 mutant or that of non-CC17-GBS (Fig. 4B), indicating that the adhesion of CC17-GBS to
224 hCMEC/D3 cells depends on Srr2- $\alpha 5\beta 1$ and Srr2- $\alpha v\beta 3$ interactions.

225 To confirm the role of $\alpha 5\beta 1$ and $\alpha v\beta 3$ integrins in CC17-GBS adhesion to hCMEC/D3, we silenced
226 the integrins expression by transfecting endothelial cells with specific siRNAs. Because integrins
227 are composed of one α chain and one β chain that combine to form heterodimers, we targeted the
228 $\alpha 5$ chain to silence $\alpha 5\beta 1$ and the $\beta 3$ chain to silence $\alpha v\beta 3$, a strategy which minimizes side effects
229 on other integrins. The effect of siRNA-mediated silencing of $\alpha 5$ or $\beta 3$ chains was efficient as
230 evidenced by Western Blot analysis (Fig. 4C and D). When $\alpha 5$ or $\beta 3$ expression was silenced,

231 CC17-GBS adhesion was significantly reduced compared with scramble control-transfected cells.
232 No additive effect was observed when both $\alpha 5$ and $\beta 3$ were simultaneously silenced. In contrast,
233 adhesion of the $\Delta srr2$ mutant strain or the non-CC17-GBS were not affected by $\alpha 5$ or $\beta 3$ integrin
234 silencing (Fig. 4E).

235 Finally, we investigated the contribution of Srr2-integrins interactions in cellular barrier crossing.
236 Indeed, bacterial adhesion to brain endothelial cells is a prerequisite for the crossing of the BBB
237 by either paracellular or transcellular mechanism. When brain microvascular endothelial cells were
238 infected with the CC17 strain for 1 h, no obvious disruption of the ZO1 tight junction protein was
239 observed (Fig. 4F). Furthermore, staining allowing to differentiate extracellular from intracellular
240 bacteria revealed the presence of intracellular bacteria suggesting a transcellular passage (Fig.
241 4F). We therefore compared the invasion by a CC17-GBS to that of the $\Delta srr2$ and non-CC17-GBS
242 strains (Fig. 4G). Invasion of the WT CC17 was higher than that of the other strains, demonstrating
243 the existence of a Srr2- dependent invasion (Fig. 4G). We thus assayed the consequences of
244 siRNA silencing of $\alpha 5$ or $\beta 3$ expression on CC17-GBS internalization. Invasion level of CC17-GBS
245 was significantly reduced in $\alpha 5$ and $\beta 3$ silenced cells (Fig. 4H). In contrast, internalizations of the
246 $\Delta srr2$ mutant and the non-CC17 GBS were unmodified (Fig. 4H). To analyze CC17-GBS
247 internalization process in hCMEC/D3, and the putative involvement of signal transduction
248 molecules involved in integrin signaling, we performed invasion assays in the presence of various
249 inhibitors. The actin-depolymerizing agent (cytochalasin D), the cholesterol-depleting agent
250 (methyl- β -cyclodextrin) and the dynamin-2 inhibitor (dynasore) inhibited CC17-GBS invasion. In
251 contrast, the microtubule-depolymerizing agent (nocodazole), the PI3Kinase inhibitor
252 (wortmannin) or the Akt inhibitor (MK22) had no effect (Fig. 4I).

253 Altogether, these results indicate that the Srr2 adhesin expressed by CC17-GBS uses $\alpha 5\beta 1$ and
254 $\alpha v\beta 3$ integrins to promote the adhesion of CC17 strains on cerebral endothelial cells, leading to
255 their internalization by a mechanism involving actin, dynamin-2 and lipid rafts.

256 ***$\alpha 5\beta 1$ and $\alpha v\beta 3$ integrins are overexpressed during the postnatal period***

257 CC17-GBS are over-represented among GBS neonatal meningitis, accounting for more than 80%
258 of the cases (4, 9, 11). In contrast, epidemiological data show that GBS is an uncommon cause
259 of meningitis in adults and CC17 is only found in 21% of the cases (37, 38). Meningeal pathogens
260 can enter the brain *via* the BBB and/or the BCSFB located in the choroid plexuses of the ventricular
261 area (12). We therefore hypothesized that neonatal susceptibility to CC17-GBS meningitis might
262 be correlated to the expression of $\alpha 5\beta 1$ and $\alpha v\beta 3$ integrins at the BBB/BCSFB level. To test this
263 hypothesis, cerebral blood vessels from neonatal and adult rats were purified and the expression
264 of $\alpha 5\beta 1$ and $\alpha v\beta 3$ was assessed by immunofluorescence staining and Western Blot analysis. A
265 striking intense $\alpha 5$ integrin staining was observed on brain vessels from pups while adult brain
266 vessels displayed a much less intense staining (Fig. 5A). Overexpression of $\alpha 5$ integrin in neonatal
267 brain vessels was confirmed by Western Blot analysis (Fig. 5B). While no $\beta 3$ expression was
268 detected on adult brain vessels, either by immunofluorescence or by Western Blot, a faint but
269 easily detectable $\beta 3$ expression was observed in brain vessels from pups rats (Fig. 5B and 5C).
270 These results indicate that $\alpha 5\beta 1$ and $\alpha v\beta 3$ integrins are overexpressed in rat brain vessels during
271 the neonatal period.

272 Choroid plexuses are composed of blood vessels which are different from those of the BBB, and
273 of stroma and choroid epithelial cells that form the BCSFB (39). Therefore, choroid plexus tissues
274 from the 4th ventricle (CP4V) or the lateral ventricles (CPLV) were collected and analyzed for $\alpha 5$
275 and $\beta 3$ expression. $\alpha 5$ integrin was found overexpressed in rats pups compared to adults, and $\beta 3$
276 integrin expression could only be detected in the choroid plexuses of rat pups (Fig.5D).

277 Importantly, similar results were obtained on human brain samples by immunohistochemistry
278 analyses of the brain of a newborn (9 days old) and an adult (52 years old), for whom the causes
279 of death were unrelated to meningitis. In the cortex, $\alpha 5$ integrin staining mainly revealed cerebral
280 blood vessels in both neonate and adult. However, the staining intensity of the cerebral blood

281 vessels was strikingly more intense in the neonatal cortex compared to the adult. $\beta 3$ expression
282 in the neonate was very faint and observed in slightly bigger blood vessels than capillaries
283 whereas it was totally absent in the adult cortex (Fig. 5E).

284 When brain sections from the ventricular area were specifically analyzed for $\alpha 5$ expression, a
285 massive staining of all choroid plexuses blood vessels was observed in the neonatal specimen
286 (Fig. 5F, arrows). In contrast and with the exception of few infiltrating cells, $\alpha 5$ expression was not
287 detected in the adult specimen (Fig. 5F arrowheads). Similar to what was observed in the cortex,
288 $\beta 3$ expression was restricted to the biggest blood vessels in pups' choroid plexuses (Fig. 5F,
289 arrows) and absent from smaller blood vessels (Fig. 5F, arrows heads) whereas it was totally
290 absent in the adult choroid plexuses (Fig. 5F). Importantly, neither $\alpha 5$ nor $\beta 3$ integrins were
291 detected in choroid plexus epithelial cells of either the neonate or the adult (Fig. 5F). Altogether,
292 these data indicate that $\alpha 5\beta 1$ and $\alpha v\beta 3$ integrins are overexpressed in human blood vessels of
293 the BBB and the BCSFB during the neonatal period.

294

295 ***Initial brain penetration of CC17-GBS occurs at the BBB and BCSFB***

296 CC17-GBS have been observed associated to both brain vessels of the BBB and choroid plexus
297 of the BCSFB in a fatal case of neonatal LOD (15). However, the initial portal of entry of GBS in
298 the brain remains unknown. To determine the initial entry site of CC17-GBS we used an *in vivo*
299 murine bacteremia-derived meningitis model (6, 16). To carry out the experiments on a more
300 amenable model than neonatal mice, we tested the presence of $\alpha 5\beta 1$ and $\alpha v\beta 3$ integrins in brain
301 vessels of juvenile mice. These integrins were also still expressed at high level in juvenile
302 compared to adult mice (Fig. 6A). Four hours after intravenous injection of juvenile mice with
303 CC17-GFP strain, bacteria were found outside the blood vessels in the cortex and the choroid
304 plexuses (Fig. 6B and C) indicating successful transmigration of CC17-GBS to the CNS at both
305 the BBB and the BCSFB.

306 ***α5β1 and αvβ3 integrins are involved in the juvenile susceptibility to CC17-GBS meningitis***

307 **in vivo**

308 Next, we studied the relevance of the interaction between Srr2 adhesin and α5β1 and αvβ3
309 integrins *in vivo*. We first controlled the ability of BR_{Srr2} to recognize murine α5β1 and αvβ3
310 integrins validating the use of the murine model (Fig. S6). We compared the susceptibility to CC17-
311 GBS meningitis of juvenile mice to that of adult mice. In order to specifically address the
312 transmigration capacity to the CNS, we adapted the experiment to have the same bacteremia in
313 juvenile and adult mice. We found that infection with 2x10⁷ CFU in juvenile and 1.5x10⁸ CFU in
314 adult mice gave similar bacteremia at 4 h pi (Fig. 7A). Four hours after intravenous infection with
315 WT bacteria, significantly less bacteria were recovered from the brain of adult mice than of juvenile
316 mice demonstrating that juvenile mice are more susceptible to CC17 meningitis than adult mice
317 (Fig. 7B). We thus assayed the requirement for the Srr2 adhesin in meningitis development in
318 juvenile and adult mice and found that significantly less Δ*srr2* than WT bacteria were recovered
319 from the brain of juvenile mice (Fig. 7B). In contrast similar bacterial counts of the WT and the
320 Δ*srr2* mutant were recovered from adult brains (Fig. 7B). Furthermore, and whereas such was not
321 the case with juvenile mice, the brain of 33 % of adult mice infected with the WT strain was free
322 of bacteria, as in Δ*srr2*-infected juvenile and adult mice (38 and 27 % respectively). These results
323 demonstrate that Srr2 adhesin contributes to the early event of CC17-GBS transmigration to the
324 CNS in juvenile mice and does not contribute to the milder CNS transmigration in adult mice.

325 We therefore addressed the role of the integrins α5β1 and αvβ3 in the Srr2-dependent
326 susceptibility of juvenile mice. To establish the contribution of integrin α5β1, and since α5-integrin-
327 KO mice are embryonically lethal (40), we developed a model based on the use of blocking
328 antibody, a strategy successfully used for other meningeal pathogens (41). Anti-α5 integrin
329 neutralizing antibody or isotype control antibody-treated mice were infected intravenously with
330 CC17-GBS. The resulting bacteremia and total CFU counts 4 hours pi in the spleen and liver were

331 similar, but significantly reduced in the brain as compared with control condition (Fig. 7C). In
332 contrast, anti- $\alpha 5$ integrin neutralizing antibody did not affect the capacity of the $\Delta srr2$ mutant to
333 reach the brain as similar bacterial counts were recovered from brain of anti- $\alpha 5$ pretreated mice
334 compared to control condition (Fig. 7D).

335 Similarly, as $\beta 3$ -integrin-KO mice suffer from vascular leakage (42), a blocking strategy was also
336 used to investigate the $\alpha v\beta 3$ integrin role in the early event of CC17-GBS transmigration to the
337 CNS. Integrin $\alpha v\beta 3$ was blocked using the mimetic peptide RGDfV which was highly efficient to
338 inhibit BR_{Srr2}- $\alpha v\beta 3$ interaction *in vitro* (Fig. 2C). RGDfV mimetic peptide or control vehicle-treated
339 mice were infected with CC17-GBS. Administration of RGDfV mimetic peptide had no effect on
340 bacteremia, spleen, and liver CFU counts 4 h pi, but decreased CC17-GBS penetration to the
341 brain compared to the control vehicle (Fig. 7E), but not that of $\Delta srr2$ mutant (Fig. 7F).

342 Together, our data demonstrate that Srr2 interaction with $\alpha 5\beta 1$ and $\alpha v\beta 3$ integrins contributes to
343 the juvenile mice susceptibility to CC17-GBS meningitis and that pre-treatments targeting these
344 integrins reduce brain invasion.

345 **DISCUSSION**

346 Neonatal bacterial meningitis is a devastating life-threatening infection of the CNS. Despite
347 antenatal screening of pregnant women associated with *intrapartum* antibiotic prophylaxis for
348 GBS-positive mothers in most high-income countries, GBS remains the leading cause of neonatal
349 meningitis. Meningitis cases due to GBS are accompanied with neurologic complications including
350 seizure, hydrocephalus, subdural empyema, or cerebrovascular diseases and lead to 10%
351 mortality and 25% permanent sequelae in surviving babies (43-45). Deciphering the mechanisms
352 that drive the initial step of brain penetration by identifying the bacterial ligands and their cognate
353 host cell receptors is of major clinical importance.

354 In our study, we demonstrate that the Srr2 adhesin, specifically and exclusively expressed by the
355 hypervirulent CC17-GBS clone, mediates bacterial binding to brain endothelial cells by interacting

356 with the cellular host receptors integrins $\alpha 5\beta 1$ and $\alpha v\beta 3$. This interaction is essential for CC17-
357 GBS to adhere and invade brain endothelial cells and contributes to meningitis development *in*
358 *vivo*. Using a simplified cellular model, we demonstrate that $\alpha 5\beta 1$ integrin is sufficient to promote
359 CC17-GBS adhesion and internalization. In contrast, although recognized by Srr2 and being
360 involved in adhesion and internalization into hCMEC/D3 and in meningitis development *in vivo*,
361 $\alpha v\beta 3$ integrin is not sufficient to trigger CC17-GBS adhesion and internalization in a cellular
362 simplified model. This indicates that $\alpha 5\beta 1$ integrin is *stricto sensu* a receptor for CC17-GBS, while
363 $\alpha v\beta 3$ integrin likely acts as a co-receptor as described for other pathogens (46). We also noticed
364 that blocking the Srr2- integrin interaction of the WT CC17 strain, by competition with soluble
365 integrins or by siRNA, did not reduce binding or invasion levels as much as deleting *srr2*. This
366 could be explained either by the fact that blocking was not 100 % efficient or by the fact that Srr2
367 could recognize other receptors than $\alpha 5\beta 1$ and $\alpha v\beta 3$. Srr2 adhesin harbors two distinct binding
368 motifs, RGD and SDV, which interact with the $\alpha v\beta 3$ integrin. While numerous bacterial adhesins
369 have been described to harbor an RGD motif, Srr2 is, to our knowledge, the first example of a
370 bacterial adhesin harboring an SDV motif which is a newly described integrin binding motif (22).
371 We have also shown, *via an in silico* approach confirmed by *in vitro* experiments, that Srr2 harbors
372 two others motifs required for direct binding to the $\alpha 5\beta 1$ integrin one in the N- and one in the C-
373 terminal sub-domain of BR_{Srr2}. We have identified FSVKI as an important motif present on N-
374 terminal domain of BR_{Srr2} for $\alpha 5\beta 1$ integrin recognition. The pathophysiological relevance for the
375 presence of two binding sites for each integrin is intriguing but has been described for other
376 bacterial adhesins, *e.g.* from Group A *Streptococcus* that possesses several integrin binding sites
377 on the same adhesin (47, 48). This probably reveals the importance of integrin recognition by
378 those pathogens in the pathophysiology of the infection.

379 Our study highlights the role of integrins in the internalization process of CC17-GBS into
380 endothelial cells. Although we did not investigate further the internalization mechanism, we found

381 that inhibitors of PI3K or Akt, that are molecules involved in integrins signaling, are not required
382 for CC17-GBS internalization; rather, CC17-GBS internalization seems to be dependent on actin
383 cytoskeleton, dynamin-2 and lipid rafts, as already described for other pathogens interacting with
384 integrins (49).

385 How recognition of integrins by Srr2 adhesin enables bacterial entry into the brain is an important
386 question that remains to be determined. On peripheral endothelial cells, bacterial adhesin-integrin
387 interactions have been shown to promote bacterial vascular transmigration (50, 51). However, our
388 current models of cerebral endothelial cells are not appropriate to investigate CC17-GBS
389 transmigration mechanism. This could occur by transcellular and/or paracellular mechanism.
390 Indeed, a transcellular crossing of the BBB has been described by Nizet *et al.* (14). But integrins
391 are also known to be interconnected to cell junctions therefore being able to affect the vascular
392 permeability in both peripheral and brain endothelial cell monolayers, which would lead to a
393 paracellular transmigration for GBS (52-56). The latter has not been described upon GBS
394 infection, yet some tight junction modifications upon GBS infection have been observed at later
395 time points than 1 h (13, 57). Although speculative, direct Srr2-integrin interaction could therefore,
396 in addition to CC17-GBS internalization in endothelial cells, lead to vascular permeability alteration
397 favoring GBS paracellular transmigration at later time points. This hypothesis is reinforced by the
398 fact that CC17-GBS strains strongly bind to fibrinogen in an Srr2-dependent manner (16, 17).
399 $\alpha 5\beta 1$ and $\alpha v\beta 3$ integrins are host receptors for fibrinogen on endothelial cells. Fibrinogen fixation
400 on its cellular receptors also leads to vascular permeability (58). Fibrinogen could therefore
401 potentiate vascular permeability by acting as a bridging molecule between CC17-GBS and
402 integrins, an indirect mechanism for integrin recognition largely employed by pathogens (59).

403 It has been previously shown that at the BBB, GBS exploits $\alpha 2\beta 1$ integrin in an indirect manner
404 through collagen recognition (60). However, collagen recognition by GBS is not a conserved
405 phenotype among GBS strains (61). This suggests that $\alpha 2\beta 1$ integrin recognition is likely not a

406 generalized mechanism to GBS strains. GBS also exploits $\alpha 1\beta 1$ integrin in the vaginal tract (27,
407 62). However, $\alpha 1\beta 1$ integrin is not expressed by brain endothelial cells (25) and we have shown
408 that neither Srr2 nor Srr1 bind $\alpha 1\beta 1$ integrin (Fig. S3).

409 Previous studies had highlighted the presence of specific CC17 surface proteins and their role in
410 CC17 neurotropism (15-17, 63). By identifying $\alpha 5\beta 1$ and $\alpha v\beta 3$ as specific receptors for Srr2, we
411 provide new insights for the understanding of the neurotropism displayed by CC17 strains
412 compared to others GBS clones. The vast majority of GBS-elicited meningitis occurs during the
413 first three months of life (64) with the overwhelming majority of cases due to the CC17 clone (4,
414 9, 11). GBS can also cause meningitis or other invasive diseases in adults particularly among the
415 elderly, those with underlying diseases or had raw fish meal. However, in adults, the CC17 clone
416 is under-represented with most of the infections due to serotype V strains or strains belonging to
417 the ST283 sequence type, the recently identified clone linked to raw fish consumption (38, 65).
418 The reasons why CC17 is overrepresented in newborns compared to adults are largely unknown.
419 We have recently shown that perinatal hormones specifically favor CC17 pathogenesis by
420 promoting the maturation of intestinal M cells responsible for intestinal translocation (6). This
421 present work reveals that $\alpha 5\beta 1/\alpha v\beta 3$ integrins are overexpressed in neonatal blood vessels of the
422 BBB and BCSFB. The overexpression of $\alpha 5\beta 1/\alpha v\beta 3$ integrins detected during the neonatal period
423 could be due to the developmental switch of integrin expression occurring during the post-natal
424 period (66). This finding is of major clinical importance as the overexpression observed during the
425 post-natal period corresponds to the peak of CC17-elicited meningitis. Finally, no expression of
426 the $\alpha 5\beta 1/\alpha v\beta 3$ integrins was detected in choroid plexus epithelial cells. Yet, CC17 bacteria have
427 been observed closely associated to CPEC on brain slices of a fatal case of LOD (15), indicating
428 that CC17 must recognize other receptors than these two integrins to cross choroid plexus
429 epithelial cells.

430 The identification of specific host receptors favoring CC17-GBS brain penetration could represent
431 useful targets for prevention and therapy of GBS meningitis. Indeed, our results show that
432 pretreatments targeting these integrins can reduce brain invasion. Receptor blockade using
433 antibodies or antagonists in adjunct treatment with antibiotics have high therapeutic potential.
434 Several anti-integrin mAbs or integrin antagonists have been already developed and are currently
435 used in various clinical or preclinical trials (67). The development of novel therapeutic strategies
436 targeting the CC17-GBS is urgent, especially because LOD cases, for which the hypervirulent
437 CC17-GBS is preponderant, have been continuously increasing over the last 20 years (10).

438

439

440 **METHODS**

441 **Bacterial strains, plasmids, primers and antibodies**

442 Bacterial strains, plasmids, primers and antibodies used in this study are listed in Table S1, S2,
443 S3 and S4 respectively. *S. agalactiae* strains were cultured in Todd Hewitt (TH) in standing filled
444 flasks broth or agar (Difco Laboratories, Detroit, MI) at 37°C. *Escherichia coli* was cultivated in
445 Luria-Bertani (LB) medium. Antibiotics were used at the following concentrations: for *E. coli*,
446 ampicillin 100 µg ml⁻¹; for *S. agalactiae*, spectinomycin 100 µg ml⁻¹.

447 **Reagents**

448 Recombinant human ICAM1 and human or mouse integrins (tested by the supplier for their ability
449 to interact with known ligands) were from R&D system. The mimetic peptides RGDfV was from
450 Sigma, RGDS and P11 were from Tocris. The Complete™ Protease inhibitor cocktail was from
451 Roche diagnostic and used following the manufacturer's instructions.

452 **Expression and purification of His-tagged-BR recombinant peptides**

453 Point mutations in putative integrin binding sites were inserted by site directed mutagenesis on
454 pET2818-BR_{Srr2} (16) using the Quick-change XL II kit (Stratagen, Netherlands). After verification
455 of the constructs by DNA sequencing, the constructed plasmids were introduced into *E. coli* BL21
456 for protein expression. Recombinant BR_{Srr2} regions were purified after induction with 1 mM of IPTG
457 using Dynabeads (Life Technologies) following manufacturer instructions.

458 **ELISA**

459 To evaluate integrin or ICAM1 binding to immobilized BR_{Srr2} or BR_{Srr1} regions, ELISA assays were
460 performed as follows: proteins were coated at 5 µg/mL overnight. After extensive wash and
461 saturation with Bovine Serum Albumin (BSA-Probumin®, Millipore), 50 µL of ligand proteins
462 (human integrins, ICAM1 or negative control BSA) were diluted at the specified concentrations in
463 PBS containing 1% of BSA (Probumin®, Millipore) and incubated 2 h at 37°C. Integrin binding
464 was assessed using antibodies listed in Table S4. Revelation was performed using OPD (Sigma)
465 or TMB (Thermofisher). Values of the negative control obtained with BSA (Probumin®, Millipore)

466 were subtracted to the signal. The effect of divalent cations on the interaction between BR_{Srr2} and
467 integrins was tested by ELISA with the same protocol as above in the presence of 1 mM Mn²⁺ or
468 1 mM Ca²⁺, as specified. Similarly, competition experiments were carried out by incubating 10 µg
469 of integrins with immobilized BR_{Srr2} in the presence of increasing concentrations of mimetic
470 peptides (RGDS, RGDfV or P11).

471 **Bioinformatic analysis**

472 *In silico* contact prediction of BR_{Srr2} (PDB code: 4MBR) interaction with α5β1 integrin (PDB code:
473 4WJK) was performed using the RaptorX Protein Complex Contact Prediction server
474 (<http://raptorx.uchicago.edu/ComplexContact/>) (28). Graphic representation of predicted contacts
475 between BR_{Srr2} and α5β1 integrin, identified by RaptorX, was generated using the PyMOL
476 Molecular Graphics System, Version 2.0 Schrödinger, LLC.

477 **Cell lines and culture conditions**

478 Human brain microvascular endothelial cells (hCMEC/D3) were cultured as described previously
479 (68). Chinese Ovary Hamster (CHO) stably transfected with human α5β1, αvβ3 or ICAM1
480 described and validated previously (30-32) were grown in DMEM containing non-essential amino
481 acids and 5% Fetal Calf Serum (FCS) in the presence of appropriate antibiotic selection pressure.
482 All cell lines were routinely tested for mycoplasma contamination (Mycoalert mycoplasma
483 detection kit, LONZA).

484 **siRNA transfection**

485 To silence the expression of α5 or β3 integrin subunits, pools of four siRNA duplexes (ON-
486 TARGET plus SMARTpool siRNA from Dharmacon) were used. The silencer select negative
487 control-1 siRNA (Ambion) was used as negative control. hCMEC/D3 were transfected with siRNA
488 using the Amaxa Nucleofactor Kit UVEC (Amaxa Biosystem) then seeded at 85 000 cells/cm² in
489 twenty-four-well plates for 24 h. Transfected cells were transfected for a second time with 25 nM
490 siRNA using Lipofectamine RNAiMAX Reagent (Invitrogen) according to the manufacturer's

491 instructions and incubated for a further 24 h. Cells were used 48 h after the first transfection.
492 Efficiency of knockdown was assessed by Western Blot analysis.

493 **Dot Blot and Western Blot analysis**

494 For Dot Blot assay, 1 µg of human α5β1, αvβ3 and ICAM1 were dotted onto PVDF membranes
495 placed in a Minifold Dot-Blot apparatus SRC-96/1 (Schleicher and Schuell). Strips were blocked
496 with PBS containing 5% skim milk for 1 h. Interaction between immobilized α5β1, αvβ3 and ICAM1
497 (negative control) and BR_{Srr2} or BR_{Srr1} was realized by incubating strips overnight at 4°C in PBS
498 containing 2% skim milk and 10 µg/ml of BR_{Srr1} or BR_{Srr2}. After incubation, the strips were washed
499 3 times in PBS Tween 0.05%, then incubated with anti-Srr2 or anti-Srr1 antibodies in 5% skim
500 milk for 1 h at room temperature. Antisera raised against Srr1 and Srr2 are highly specific and
501 display similar affinity (16).

502 For Western Blot, protein concentration was determined using the BCA protein assay kit
503 (Thermoscientific). Proteins were separated by SDS-PAGE then transferred to PVDF membrane
504 using the Trans-Blot Turbo transfer pack (Bio-Rad). Membranes were blocked in PBS containing
505 5% skimmed milk and incubated for 1 h with primary antibodies. Anti-actin directly coupled to HRP
506 was used as a loading control for Western Blot.

507 After washing and incubation with HRP-conjugated secondary antibody (Jackson
508 Immunoresearch West Grove, PA), strips from Dot Blot or membranes from Western Blot were
509 revealed using the ECL detection system (Perkin-Elmer) and signals were detected using the
510 chemiluminescence imaging system (Fusion, Vilber-Lourmat).

511 **Association and invasion assays**

512 Bacterial adhesion or invasion assays were performed in cellular culture media without FCS at a
513 multiplicity of infection (MOI) of 10 bacteria per cell unless otherwise specified. Briefly, bacteria
514 were grown to the mid-log phase, washed twice with sterile PBS then added to cells and
515 centrifuged 5 min at 211g to synchronize infection. After 1 h of incubation at 37°C under a 5% CO₂
516 atmosphere, monolayers were washed 4 times with PBS. Cell-association was determined after

517 lysis with sterile H₂O. Appropriate dilutions were made in sterile PBS, then plated on TH agar and
518 colony forming units (CFU) counted. The percent of association was calculated as follows: (CFU
519 on plate count / CFU in inoculum) × 100. Assays were performed in triplicate and were repeated
520 at least three times. When specified, results were expressed as normalized to the control
521 condition.

522 For invasion assay 1 h-infected cell monolayers were treated for 30 min with cellular culture media
523 containing penicillin/streptomycin (Gibco) and gentamicin (200 µg/ml) to kill extracellular bacteria.
524 The monolayers were washed twice with PBS, and lysed with sterile H₂O. Appropriate dilutions
525 were plated on TH agar and CFUs counted. The percent of invasion was calculated as follows:
526 (CFU on plate count / CFU in inoculum) × 100. Assays were performed in triplicate and were
527 repeated at least three times. When specified, results were expressed as normalized to the control
528 condition. To decipher host signaling pathways during CC17-GBS internalization, hCMEC/D3 cells
529 were pretreated with cytochalasin D (2µM), nocodazole (1µM), wortmannin (100nM), MK2206
530 (2µM), Methyl-β-cyclodextrin (2.5mM) or dynasore (80µM) for 1 h prior infection with CC17-GBS.
531 Inhibitors were left during the time of infection at the same concentration except for dynasore for
532 which concentration was dropped to 10µM. Treatments did not affect bacterial or cell viability (data
533 not shown).

534 **Immunofluorescent staining and image analysis**

535 hCMEC/D3 cells were grown on Thermanox coverslips (Thermo Fischer Scientific). Isolated brain
536 microvessels were stucked to slides using Cell Tak (Corning). Infected or non-infected cells or
537 isolated brain microvessels were fixed in PBS containing 4% paraformaldehyde (PFA) for 10 min.
538 Following fixation, samples were permeabilized by incubation in PBS containing 0.1% Triton-X100
539 for 4 min at room temperature then blocked for at least 1 h at room temperature in PBS containing
540 10% serum. Primary antibodies, diluted in 10% serum-PBS, were incubated for at least 1 h at
541 room temperature. After 3 washes with PBS, samples were incubated for 1 h at room temperature
542 with conjugated-secondary's antibodies (Jackson ImmunoResearch Laboratories) diluted in PBS

543 containing 10% serum. DAPI was used to counter-stain nuclei; phalloidin-633 or 594 to stain actin
544 and isolectin B4-FITC to counter-stain microvessels. After 3 washes in PBS, coverslips were
545 mounted in DAKO fluorescent mounting media (DAKO). Image acquisitions were realized using
546 confocal laser scanning microscopy (Leica DMI6000) coupled to a spinning disk confocal head
547 (YokogawaCSU-X1M1), controlled by the Metamorph 7.7.5 software. Images were processed
548 using the ImageJ software.

549 To discriminate between extracellular and intracellular bacteria, cells were infected with GFP
550 expressing bacteria. Extracellular GFP-expressing bacteria were counterstained in
551 unpermeabilized conditions with an anti-GBS serum followed by a secondary rhodamine
552 isothiocyanate-labeled antibody. Under these conditions, extracellular bacteria were green (GFP-
553 labeled bacteria) and decorated with red (anti-GBS labeling), whereas intracellular bacteria were
554 solely green (GFP-labeled bacteria).

555 **Mechanical isolation of brain microvessels**

556 Brain vessels from neonatal (2 days old), juvenile (3 weeks old) or adult (3 months old) rat or mice
557 were isolated as described previously (69). Briefly, brains were collected, and triturated in a Potter-
558 Thomas homogenizer. The homogenate was centrifuged and the pellet was resuspended in buffer
559 containing 18% dextran. After centrifugation, myelin was eliminated and the pellet containing
560 cerebral vessels was resuspended in a buffer containing 1% BSA. This suspension was filtered
561 on a 20 µm Nylon Net filter and vessels fragments were recovered from the filter in a buffer
562 containing 1% BSA. After final centrifugation, pellets of cerebral vessels were snap-frozen and
563 kept at -80°C until used for Western Blot analysis or fixed to glass slides for immunofluorescence
564 using Cell Tak (Corning).

565 **Collection of lateral and 4th Ventricular Choroid Plexus**

566 Choroid plexuses of both lateral and 4th ventricles dissected from neonatal (2-day-old) and adult
567 rats under a stereomicroscope, as previously described, were provided by the Brain Interface

568 exploratory Platform (BIP, CRNL, Lyon, France) (70). The collected tissues were snap-frozen and
569 kept at -80°C until used.

570 **Immunohistochemistry**

571 Immunohistochemistry was performed by the Cochin HistIM Facility (Histology, Immunostaining,
572 laser, Microdissection). The paraffin embedded brain sections were cleared before incubation in
573 citrate buffer (pH 6.0). Expression of $\alpha 5$ or $\beta 3$ integrin on sections was detected using the Bond
574 Polymer Refine Detection (Leica) kit with specific antibodies for $\alpha 5$ or $\beta 3$ integrins and the
575 Immunostaining automaton (Bond III, Leica). Pictures were acquired using the slide scanner
576 (Lamina, Perkin Elmer).

577 **Animal experiments**

578 Juvenile (3 weeks old) and adult (3 months old) BALB/c mice were infected by intravenous
579 injection with 2×10^7 and 1.5×10^8 CFU respectively of exponentially growing GBS strains for 4 h.
580 For some experiments, juvenile mice were pretreated by injecting intravenously either 10 μg of
581 anti- $\alpha 5$ antibodies or isotype control, 5 mg/kg cyclic mimetic peptide RGDfV or PBS one hour
582 before challenge. No side effects in mice were observed following pre-treatment targeting $\alpha 5\beta 1$
583 or $\alpha v\beta 3$ integrins. After 4 h of infection, mice were sacrificed, and, blood, spleen, liver and brain
584 were collected. The brain and spleen were homogenized in 1 mL of 0.9% sodium chloride using
585 a tissue homogenizer (Precellys system, Bertin Technologies) and liver were homogeneized in 9
586 mL using an Ultraturax. Serial dilutions in 0.9% sodium chloride were immediately plated on TH
587 agar for CFU counts. Bacterial counts in the brains were corrected for blood contamination using
588 the bacterial burden in the bloodstream and a conservative estimate of the mouse cerebral blood
589 volume of 2.5 ml per g tissue as described previously (71).

590 To study the portal of entry into the brain of CC17-GBS, juvenile mice were perfused and brains
591 were recovered and fixed overnight in PFA. The brains were embedded in 5% agarose and cut
592 into 500 μm -thick sections using a vibratome (Leica). The brain sections were clarified using Ethyl
593 cinnamate (Eci) (72) and immunostained using anti-CD31 (a marker for capillaries) and anti-

594 transthyretin (TTR, a marker for choroid plexuses) antibodies. The tissue sections were imaged
595 using a Xplore Spinning confocal microscope. Images were processed using the ImageJ software.

596 **Statistical analysis**

597 All assays were performed at least in three independent experiments. Data represent mean \pm
598 SEM and statistical analyses were performed using GraphPad Prism 5.0 (GraphPad Software,
599 San Diego, California). Significance levels were set at $*p \leq 0.05$; $**p \leq 0.01$; $***p \leq 0.001$.

600 **Study approval**

601 Written informed consent was obtained for all human samples used in this study.

602 All animal experiments described in this study were conducted in accordance with the guidelines
603 of Paris Descartes University, in compliance with the European animal welfare regulation
604 (http://ec.europa.eu/environment/chemicals/lab_animals/home_en.html) and were approved by
605 the Institut Cochin University Paris Descartes animal care and use committee (CEEA34;
606 Agreement number 2018021616168438).

607 **AUTHOR CONTRIBUTIONS:**

608 JG designed the research. RDDC, AP, ASB, CA, CC, AB, LC, and JG performed the experiments.
609 GB performed *in silico* analysis of BR_{Srr2}- $\alpha 5\beta 1$ interaction. IP and CR provided anatomical pieces
610 of human brain. ACB, MCS and JG performed brain microvessels purification. JG, RDDC, AP, AF
611 analyzed the data. AF, AT, CP, EF and CAR provided intellectual input and guidance. JG wrote
612 the manuscript and AF, AT, CP contributed to finalizing the manuscript. All authors discussed
613 results and reviewed the final version of the manuscript.

614 **ACKNOWLEDGMENTS**

615 We are grateful to Pierre-Olivier Couraud (INSERM, Paris, France) for the gift of hCMEC/D3 cells,
616 Alain Duperray for the gift of CHO-ICAM1 cells, Yoshikazu Takada for the gift of CHO- $\alpha v\beta 3$ cells
617 and Glen Ulett for the gift of the GFP plasmid. We are extremely grateful to Nathalie Strazielle and
618 Jean-François Gherzi-Egea from Blood/brain Interfaces exploratory Platform (BIP, CRNL, Lyon,

619 France, <https://crnl.univ-lyon1.fr/index.php/en/Resource/Platforms/BIP>) for choroid plexus
620 isolation and helpful comments. We thank Matthieu Benard from the animal facility of the Institut
621 Cochin and Marine Gaillard for their help with animal experiments and Thomas Guilbert and
622 Fabienne Regnier for their help with brain slices clarification. We also thank the Imag'IC and HistIM
623 core facilities of the Cochin Institute and Shaynoor Dramsi for anti-Srr1 antibody and for critical
624 reading of the manuscript.

625

626 **FINANCIAL SUPPORT**

627 This work was supported by Agence Nationale de la Recherche (ANR) (Grant StrepB2brain, ANR-
628 17-CE15-0026-01). LC is a recipient of a post-doctoral fellowship from the ANR (StrepB2brain).
629 ASB is a doctoral fellow funded by Université de Paris. RDDC was funded by FERCM.

630

631 **REFERENCES**

- 632 1. Da Cunha, V., Davies, M.R., Douarre, P.E., Rosinski-Chupin, I., Margarit, I., Spinali, S.,
633 Perkins, T., Lechat, P., Dmytruk, N., Sauvage, E., et al. 2014. Streptococcus agalactiae clones
634 infecting humans were selected and fixed through the extensive use of tetracycline. *Nat Commun*
635 5:4544.
- 636 2. Russell, N.J., Seale, A.C., O'Driscoll, M., O'Sullivan, C., Bianchi-Jassir, F., Gonzalez-
637 Guarin, J., Lawn, J.E., Baker, C.J., Bartlett, L., Cutland, C., et al. 2017. Maternal Colonization With
638 Group B Streptococcus and Serotype Distribution Worldwide: Systematic Review and Meta-
639 analyses. *Clin Infect Dis* 65:S100-S111.
- 640 3. Edwards, M., Nizet, V., and Baker, C.J. 2011. CHAPTER 12 - Group B Streptococcal
641 Infections. *Infectious Diseases of the Fetus and Newborn (Seventh Edition)*
642 419-469.

- 643 4. Joubrel, C., Tazi, A., Six, A., Dmytruk, N., Touak, G., Bidet, P., Raymond, J., Trieu Cuot,
644 P., Fouet, A., Kerneis, S., et al. 2015. Group B streptococcus neonatal invasive infections, France
645 2007-2012. *Clin Microbiol Infect* 21:910-916.
- 646 5. Morinis, J., Shah, J., Murthy, P., and Fulford, M. 2011. Horizontal transmission of group B
647 streptococcus in a neonatal intensive care unit. *Paediatr Child Health* 16:e48-50.
- 648 6. Hays, C., Touak, G., Bouaboud, A., Fouet, A., Guignot, J., Poyart, C., and Tazi, A. 2019.
649 Perinatal hormones favor CC17 group B Streptococcus intestinal translocation through M cells
650 and hypervirulence in neonates. *Elife* 8.
- 651 7. Tazi, A., Plainvert, C., Anselem, O., Ballon, M., Marcou, V., Seco, A., El Alaoui, F., Joubrel,
652 C., El Helali, N., Falloukh, E., et al. 2019. Risk Factors for Infant Colonization by Hypervirulent
653 CC17 Group B Streptococcus: Toward the Understanding of Late-onset Disease. *Clin Infect Dis*.
- 654 8. Lamy, M.C., Dramsi, S., Billoet, A., Reglier-Poupet, H., Tazi, A., Raymond, J., Guerin, F.,
655 Couve, E., Kunst, F., Glaser, P., et al. 2006. Rapid detection of the "highly virulent" group B
656 Streptococcus ST-17 clone. *Microbes Infect* 8:1714-1722.
- 657 9. Manning, S.D., Springman, A.C., Lehotzky, E., Lewis, M.A., Whittam, T.S., and Davies,
658 H.D. 2009. Multilocus sequence types associated with neonatal group B streptococcal sepsis and
659 meningitis in Canada. *J Clin Microbiol* 47:1143-1148.
- 660 10. Romain, A.S., Cohen, R., Plainvert, C., Joubrel, C., Bechet, S., Perret, A., Tazi, A., Poyart,
661 C., and Levy, C. 2018. Clinical and Laboratory Features of Group B Streptococcus Meningitis in
662 Infants and Newborns: Study of 848 Cases in France, 2001-2014. *Clin Infect Dis* 66:857-864.
- 663 11. Seale, A.C., Koech, A.C., Sheppard, A.E., Barsosio, H.C., Langat, J., Anyango, E.,
664 Mwakio, S., Mwarumba, S., Morpeth, S.C., Anampiu, K., et al. 2016. Maternal colonization with
665 Streptococcus agalactiae and associated stillbirth and neonatal disease in coastal Kenya. *Nat*
666 *Microbiol* 1:16067.
- 667 12. Coureuil, M., Lecuyer, H., Bourdoulous, S., and Nassif, X. 2017. A journey into the brain:
668 insight into how bacterial pathogens cross blood-brain barriers. *Nat Rev Microbiol* 15:149-159.

- 669 13. Kim, B.J., Hancock, B.M., Bermudez, A., Del Cid, N., Reyes, E., van Sorge, N.M., Lauth,
670 X., Smurthwaite, C.A., Hilton, B.J., Stotland, A., et al. 2015. Bacterial induction of Snail1
671 contributes to blood-brain barrier disruption. *J Clin Invest* 125:2473-2483.
- 672 14. Nizet, V., Kim, K.S., Stins, M., Jonas, M., Chi, E.Y., Nguyen, D., and Rubens, C.E. 1997.
673 Invasion of brain microvascular endothelial cells by group B streptococci. *Infect Immun* 65:5074-
674 5081.
- 675 15. Tazi, A., Disson, O., Bellais, S., Bouaboud, A., Dmytruk, N., Dramsi, S., Mistou, M.Y.,
676 Khun, H., Mechler, C., Tardieux, I., et al. 2010. The surface protein HvgA mediates group B
677 streptococcus hypervirulence and meningeal tropism in neonates. *J Exp Med* 207:2313-2322.
- 678 16. Six, A., Bellais, S., Bouaboud, A., Fouet, A., Gabriel, C., Tazi, A., Dramsi, S., Trieu-Cuot,
679 P., and Poyart, C. 2015. Srr2, a multifaceted adhesin expressed by ST-17 hypervirulent Group B
680 Streptococcus involved in binding to both fibrinogen and plasminogen. *Mol Microbiol* 97:1209-
681 1222.
- 682 17. Seo, H.S., Minasov, G., Seepersaud, R., Doran, K.S., Dubrovskaya, I., Shuvalova, L.,
683 Anderson, W.F., Iverson, T.M., and Sullam, P.M. 2013. Characterization of fibrinogen binding by
684 glycoproteins Srr1 and Srr2 of Streptococcus agalactiae. *J Biol Chem* 288:35982-35996.
- 685 18. Seo, H.S., Mu, R., Kim, B.J., Doran, K.S., and Sullam, P.M. 2012. Binding of glycoprotein
686 Srr1 of Streptococcus agalactiae to fibrinogen promotes attachment to brain endothelium and the
687 development of meningitis. *PLoS Pathog* 8:e1002947.
- 688 19. Wang, N.Y., Patras, K.A., Seo, H.S., Cavaco, C.K., Rosler, B., Neely, M.N., Sullam, P.M.,
689 and Doran, K.S. 2014. Group B streptococcal serine-rich repeat proteins promote interaction with
690 fibrinogen and vaginal colonization. *J Infect Dis* 210:982-991.
- 691 20. Bang, J.Y., Kim, E.Y., Kang, D.K., Chang, S.I., Han, M.H., Baek, K.H., and Kang, I.C. 2011.
692 Pharmacoproteomic analysis of a novel cell-permeable peptide inhibitor of tumor-induced
693 angiogenesis. *Mol Cell Proteomics* 10:M110 005264.

- 694 21. Ruoslahti, E. 1996. RGD and other recognition sequences for integrins. *Annu Rev Cell*
695 *Dev Biol* 12:697-715.
- 696 22. Choi, Y., Kim, E., Lee, Y., Han, M.H., and Kang, I.C. 2010. Site-specific inhibition of integrin
697 alpha v beta 3-vitronectin association by a ser-asp-val sequence through an Arg-Gly-Asp-binding
698 site of the integrin. *Proteomics* 10:72-80.
- 699 23. Hynes, R.O., Lively, J.C., McCarty, J.H., Taverna, D., Francis, S.E., Hovalala-Dilke, K.,
700 and Xiao, Q. 2002. The diverse roles of integrins and their ligands in angiogenesis. *Cold Spring*
701 *Harb Symp Quant Biol* 67:143-153.
- 702 24. Paulus, W., Baur, I., Schuppan, D., and Roggendorf, W. 1993. Characterization of integrin
703 receptors in normal and neoplastic human brain. *Am J Pathol* 143:154-163.
- 704 25. Wang, J., and Milner, R. 2006. Fibronectin promotes brain capillary endothelial cell survival
705 and proliferation through alpha5beta1 and alphavbeta3 integrins via MAP kinase signalling. *J*
706 *Neurochem* 96:148-159.
- 707 26. Zhang, K., and Chen, J. 2012. The regulation of integrin function by divalent cations. *Cell*
708 *Adh Migr* 6:20-29.
- 709 27. Bolduc, G.R., and Madoff, L.C. 2007. The group B streptococcal alpha C protein binds
710 alpha1beta1-integrin through a novel KTD motif that promotes internalization of GBS within human
711 epithelial cells. *Microbiology* 153:4039-4049.
- 712 28. Zeng, H., Wang, S., Zhou, T., Zhao, F., Li, X., Wu, Q., and Xu, J. 2018. ComplexContact:
713 a web server for inter-protein contact prediction using deep learning. *Nucleic Acids Res* 46:W432-
714 W437.
- 715 29. Schreiner, C.L., Bauer, J.S., Danilov, Y.N., Hussein, S., Sczekan, M.M., and Juliano, R.L.
716 1989. Isolation and characterization of Chinese hamster ovary cell variants deficient in the
717 expression of fibronectin receptor. *J Cell Biol* 109:3157-3167.

- 718 30. Guignot, J., Hudault, S., Kansau, I., Chau, I., and Servin, A.L. 2009. Human decay-
719 accelerating factor and CEACAM receptor-mediated internalization and intracellular lifestyle of
720 Afa/Dr diffusely adhering Escherichia coli in epithelial cells. *Infect Immun* 77:517-531.
- 721 31. Takagi, J., Kamata, T., Meredith, J., Puzon-McLaughlin, W., and Takada, Y. 1997.
722 Changing ligand specificities of alphavbeta1 and alphavbeta3 integrins by swapping a short
723 diverse sequence of the beta subunit. *J Biol Chem* 272:19794-19800.
- 724 32. Sans, E., Delachanal, E., and Duperray, A. 2001. Analysis of the roles of ICAM-1 in
725 neutrophil transmigration using a reconstituted mammalian cell expression model: implication of
726 ICAM-1 cytoplasmic domain and Rho-dependent signaling pathway. *J Immunol* 166:544-551.
- 727 33. Bhattacharya, S., Ying, X., Fu, C., Patel, R., Kuebler, W., Greenberg, S., and
728 Bhattacharya, J. 2000. alpha(v)beta(3) integrin induces tyrosine phosphorylation-dependent
729 Ca(2+) influx in pulmonary endothelial cells. *Circ Res* 86:456-462.
- 730 34. Conforti, G., Dominguez-Jimenez, C., Zanetti, A., Gimbrone, M.A., Jr., Cremona, O.,
731 Marchisio, P.C., and Dejana, E. 1992. Human endothelial cells express integrin receptors on the
732 luminal aspect of their membrane. *Blood* 80:437-446.
- 733 35. Singh, B., Fu, C., and Bhattacharya, J. 2000. Vascular expression of the alpha(v)beta(3)-
734 integrin in lung and other organs. *Am J Physiol Lung Cell Mol Physiol* 278:L217-226.
- 735 36. Xanthis, I., Souilhol, C., Serbanovic-Canic, J., Roddie, H., Kalli, A.C., Fragiadaki, M.,
736 Wong, R., Shah, D.R., Askari, J.A., Canham, L., et al. 2019. beta1 integrin is a sensor of blood
737 flow direction. *J Cell Sci* 132.
- 738 37. van Kassel, M.N., Bijlsma, M.W., Brouwer, M.C., van der Ende, A., and van de Beek, D.
739 2019. Community-acquired group B streptococcal meningitis in adults: 33 cases from prospective
740 cohort studies. *J Infect* 78:54-57.
- 741 38. Luan, S.L., Granlund, M., Sellin, M., Lagergard, T., Spratt, B.G., and Norgren, M. 2005.
742 Multilocus sequence typing of Swedish invasive group B streptococcus isolates indicates a
743 neonatally associated genetic lineage and capsule switching. *J Clin Microbiol* 43:3727-3733.

744 39. Strazielle, N., and Gherzi-Egea, J.F. 2000. Choroid plexus in the central nervous system:
745 biology and physiopathology. *J Neuropathol Exp Neurol* 59:561-574.

746 40. Yang, J.T., Rayburn, H., and Hynes, R.O. 1993. Embryonic mesodermal defects in alpha
747 5 integrin-deficient mice. *Development* 119:1093-1105.

748 41. Iovino, F., Engelen-Lee, J.Y., Brouwer, M., van de Beek, D., van der Ende, A., Valls Seron,
749 M., Mellroth, P., Muschiol, S., Bergstrand, J., Widengren, J., et al. 2017. pIgR and PECAM-1 bind
750 to pneumococcal adhesins RrgA and PspC mediating bacterial brain invasion. *J Exp Med*
751 214:1619-1630.

752 42. Su, G., Atakilit, A., Li, J.T., Wu, N., Bhattacharya, M., Zhu, J., Shieh, J.E., Li, E., Chen, R.,
753 Sun, S., et al. 2012. Absence of integrin alphavbeta3 enhances vascular leak in mice by inhibiting
754 endothelial cortical actin formation. *Am J Respir Crit Care Med* 185:58-66.

755 43. Tibussek, D., Sinclair, A., Yau, I., Teatero, S., Fittipaldi, N., Richardson, S.E., Mayatepek,
756 E., Jahn, P., and Askalan, R. 2015. Late-onset group B streptococcal meningitis has
757 cerebrovascular complications. *J Pediatr* 166:1187-1192 e1181.

758 44. Kohli-Lynch, M., Russell, N.J., Seale, A.C., Dangor, Z., Tann, C.J., Baker, C.J., Bartlett,
759 L., Cutland, C., Gravett, M.G., Heath, P.T., et al. 2017. Neurodevelopmental Impairment in
760 Children After Group B Streptococcal Disease Worldwide: Systematic Review and Meta-analyses.
761 *Clin Infect Dis* 65:S190-S199.

762 45. Andrade, E.B., Magalhaes, A., Puga, A., Costa, M., Bravo, J., Portugal, C.C., Ribeiro, A.,
763 Correia-Neves, M., Faustino, A., Firon, A., et al. 2018. A mouse model reproducing the
764 pathophysiology of neonatal group B streptococcal infection. *Nat Commun* 9:3138.

765 46. Wang, X., Huang, D.Y., Huong, S.M., and Huang, E.S. 2005. Integrin alphavbeta3 is a
766 coreceptor for human cytomegalovirus. *Nat Med* 11:515-521.

767 47. Humtsoe, J.O., Kim, J.K., Xu, Y., Keene, D.R., Hook, M., Lukomski, S., and Wary, K.K.
768 2005. A streptococcal collagen-like protein interacts with the alpha2beta1 integrin and induces
769 intracellular signaling. *J Biol Chem* 280:13848-13857.

- 770 48. Weckel, A., Ahamada, D., Bellais, S., Mehats, C., Plainvert, C., Longo, M., Poyart, C., and
771 Fouet, A. 2018. The N-terminal domain of the R28 protein promotes emm28 group A
772 Streptococcus adhesion to host cells via direct binding to three integrins. *J Biol Chem* 293:16006-
773 16018.
- 774 49. Gianni, T., Gatta, V., and Campadelli-Fiume, G. 2010. α V β 3-integrin routes
775 herpes simplex virus to an entry pathway dependent on cholesterol-rich lipid rafts and dynamin2.
776 *Proc Natl Acad Sci U S A* 107:22260-22265.
- 777 50. Kumar, D., Ristow, L.C., Shi, M., Mukherjee, P., Caine, J.A., Lee, W.Y., Kubes, P., Coburn,
778 J., and Chaconas, G. 2015. Intravital Imaging of Vascular Transmigration by the Lyme Spirochete:
779 Requirement for the Integrin Binding Residues of the *B. burgdorferi* P66 Protein. *PLoS Pathog*
780 11:e1005333.
- 781 51. Ristow, L.C., Bonde, M., Lin, Y.P., Sato, H., Curtis, M., Wesley, E., Hahn, B.L., Fang, J.,
782 Wilcox, D.A., Leong, J.M., et al. 2015. Integrin binding by *Borrelia burgdorferi* P66 facilitates
783 dissemination but is not required for infectivity. *Cell Microbiol* 17:1021-1036.
- 784 52. Alghisi, G.C., Ponsonnet, L., and Ruegg, C. 2009. The integrin antagonist cilengitide
785 activates α V β 3, disrupts VE-cadherin localization at cell junctions and enhances
786 permeability in endothelial cells. *PLoS One* 4:e4449.
- 787 53. Engelhardt, B. 2011. β 1-integrin/matrix interactions support blood-brain barrier integrity.
788 *J Cereb Blood Flow Metab* 31:1969-1971.
- 789 54. Hermann, D.M., and ElAli, A. 2012. The abluminal endothelial membrane in neurovascular
790 remodeling in health and disease. *Sci Signal* 5:re4.
- 791 55. Osada, T., Gu, Y.H., Kanazawa, M., Tsubota, Y., Hawkins, B.T., Spatz, M., Milner, R., and
792 del Zoppo, G.J. 2011. Interendothelial claudin-5 expression depends on cerebral endothelial cell-
793 matrix adhesion by β (1)-integrins. *J Cereb Blood Flow Metab* 31:1972-1985.
- 794 56. Pulous, F.E., and Petrich, B.G. 2019. Integrin-dependent regulation of the endothelial
795 barrier. *Tissue Barriers* 7:1685844.

- 796 57. Kim, B.J., Bee, O.B., McDonagh, M.A., Stebbins, M.J., Palecek, S.P., Doran, K.S., and
797 Shusta, E.V. 2017. Modeling Group B Streptococcus and Blood-Brain Barrier Interaction by Using
798 Induced Pluripotent Stem Cell-Derived Brain Endothelial Cells. *mSphere* 2.
- 799 58. Davalos, D., and Akassoglou, K. 2012. Fibrinogen as a key regulator of inflammation in
800 disease. *Semin Immunopathol* 34:43-62.
- 801 59. Hauck, C.R., Borisova, M., and Muenzner, P. 2012. Exploitation of integrin function by
802 pathogenic microbes. *Curr Opin Cell Biol* 24:637-644.
- 803 60. Banerjee, A., Kim, B.J., Carmona, E.M., Cutting, A.S., Gurney, M.A., Carlos, C., Feuer, R.,
804 Prasadarao, N.V., and Doran, K.S. 2011. Bacterial Pili exploit integrin machinery to promote
805 immune activation and efficient blood-brain barrier penetration. *Nat Commun* 2:462.
- 806 61. Dramsi, S., Morello, E., Poyart, C., and Trieu-Cuot, P. 2012. Epidemiologically and
807 clinically relevant Group B Streptococcus isolates do not bind collagen but display enhanced
808 binding to human fibrinogen. *Microbes Infect* 14:1044-1048.
- 809 62. Vornhagen, J., Armistead, B., Santana-Ufret, V., Gendrin, C., Merillat, S., Coleman, M.,
810 Quach, P., Boldenow, E., Alishetti, V., Leonhard-Melief, C., et al. 2018. Group B streptococcus
811 exploits vaginal epithelial exfoliation for ascending infection. *J Clin Invest* 128:1985-1999.
- 812 63. Brochet, M., Couve, E., Zouine, M., Vallaey, T., Rusniok, C., Lamy, M.C., Buchrieser, C.,
813 Trieu-Cuot, P., Kunst, F., Poyart, C., et al. 2006. Genomic diversity and evolution within the
814 species *Streptococcus agalactiae*. *Microbes Infect* 8:1227-1243.
- 815 64. Phares, C.R., Lynfield, R., Farley, M.M., Mohle-Boetani, J., Harrison, L.H., Petit, S., Craig,
816 A.S., Schaffner, W., Zansky, S.M., Gershman, K., et al. 2008. Epidemiology of invasive group B
817 streptococcal disease in the United States, 1999-2005. *JAMA* 299:2056-2065.
- 818 65. Kalimuddin, S., Chen, S.L., Lim, C.T.K., Koh, T.H., Tan, T.Y., Kam, M., Wong, C.W.,
819 Mehershahi, K.S., Chau, M.L., Ng, L.C., et al. 2017. 2015 Epidemic of Severe *Streptococcus*
820 *agalactiae* Sequence Type 283 Infections in Singapore Associated With the Consumption of Raw

821 Freshwater Fish: A Detailed Analysis of Clinical, Epidemiological, and Bacterial Sequencing Data.
822 *Clin Infect Dis* 64:S145-S152.

823 66. Milner, R., and Campbell, I.L. 2002. Developmental regulation of beta1 integrins during
824 angiogenesis in the central nervous system. *Mol Cell Neurosci* 20:616-626.

825 67. Raab-Westphal, S., Marshall, J.F., and Goodman, S.L. 2017. Integrins as Therapeutic
826 Targets: Successes and Cancers. *Cancers (Basel)* 9.

827 68. Weksler, B., Romero, I.A., and Couraud, P.O. 2013. The hCMEC/D3 cell line as a model
828 of the human blood brain barrier. *Fluids Barriers CNS* 10:16.

829 69. Boulay, A.C., Saubamea, B., Decleves, X., and Cohen-Salmon, M. 2015. Purification of
830 Mouse Brain Vessels. *J Vis Exp*:e53208.

831 70. Kratzer, I., Liddelow, S.A., Saunders, N.R., Dziegielewska, K.M., Strazielle, N., and Ghersi-
832 Egea, J.F. 2013. Developmental changes in the transcriptome of the rat choroid plexus in relation
833 to neuroprotection. *Fluids Barriers CNS* 10:25.

834 71. Doran, K.S., Liu, G.Y., and Nizet, V. 2003. Group B streptococcal beta-hemolysin/cytolysin
835 activates neutrophil signaling pathways in brain endothelium and contributes to development of
836 meningitis. *J Clin Invest* 112:736-744.

837 72. Vigouroux, R.J, Belle, M., and Chédotal, A. 2017. Neuroscience in the third dimension:
838 shedding new light on the brain with tissue clearing. *Mol. Brain* 10:33

839

840

841 **FIGURE LEGENDS**

842 **Figure 1: BR_{Srr2} recognizes $\alpha 5\beta 1$ and $\alpha v\beta 3$ integrins in a direct manner.** (A) Schematic
843 representation of Srr2 and Srr1 proteins with signal sequence (checkered), serine-rich regions
844 (white), LPxTG cell wall anchoring motif (hatched) and the binding regions of Srr2 (black) or Srr1
845 (grey) delineated by dashed lines. Numbers in black indicate the position of amino acid residues
846 and letters in white indicate the predicted motifs of interaction with integrins. (B) Dot Blotting was
847 performed to determine the interaction between immobilized human $\alpha 5\beta 1$, $\alpha v\beta 3$ integrins or
848 ICAM1 and BR_{Srr2} or BR_{Srr1}. Purified BR_{Srr2} and BR_{Srr1} proteins are shown in Fig. S1A. (C, D and
849 E) Interaction of BR_{Srr2} (black squares) or BR_{Srr1} (grey circles) with human $\alpha 5\beta 1$ integrin (C), $\alpha v\beta 3$
850 integrin (D) or ICAM1 (E) were assessed by ELISA. Results were normalized to negative control
851 (BSA). Statistical analysis: data shown are mean \pm SEM of at least three independent
852 experiments. Two-Way ANOVA with Bonferroni's multiple comparisons post-test was performed.
853 NS, non-significant; *, $p < 0.05$; **, $p < 0.01$; ***, $p < 0.001$.

854 **Figure 2: Identification of BR_{Srr2} residues involved in the direct interaction with $\alpha v\beta 3$ and**
855 **$\alpha 5\beta 1$ integrins.** (A and B) Interaction of BR_{Srr2}, or its mutated forms, with integrins $\alpha v\beta 3$ (A) or
856 $\alpha 5\beta 1$ (B) were assessed by ELISA. Mutated forms of BR_{Srr2} proteins are shown in Supplementary
857 Fig. S1B and C. (C and D) Interaction of BR_{Srr2} with integrins $\alpha v\beta 3$ (C) or $\alpha 5\beta 1$ (D) in the presence
858 of increasing concentration of mimetic peptides were assessed by ELISA. Results were expressed
859 as % of untreated condition. (E) Graphic representation of predicted contacts between BR_{Srr2} and
860 $\alpha 5\beta 1$ integrin identified by RaptorX (Fig. S4). RaptorX mapped on the $\alpha 5$ (grey) $\beta 1$ (green) integrin
861 subunits predicted two contact zones located in the N-terminal (blue) and C-terminal (gold)
862 domains of BR_{Srr2}. Only the most reliable contacts (contact probability >0.7) are depicted as yellow
863 lines in the scheme. (F) Schematic representation of BR_{Srr2} or its truncated forms. Numbers in
864 black indicate the position of amino acid residues in Srr2, and letters in white the predicted motifs
865 of interaction with the integrin $\alpha 5\beta 1$. (G) ELISA assays with integrin $\alpha 5\beta 1$ were performed using
866 equimolar amounts of coated BR_{Srr2} or of its truncated forms. (H) Interaction of BR_{Srr2}, or its

867 mutated forms, with the integrin $\alpha 5\beta 1$ were assessed by ELISA. Mutated forms of BR_{Srr2} proteins
868 are shown in Fig. S1D and E.

869 ELISA results were normalized to the negative control (BSA). Statistical analysis: data shown are
870 mean \pm SEM of at least three independent experiments. Two-Way ANOVA with Bonferroni's
871 multiple comparisons post-test was performed. NS, non-significant; *, $p < 0.05$; **, $p < 0.01$; ***, p
872 < 0.001 .

873 **Figure 3: $\alpha 5\beta 1$ promotes adhesion and invasion of CC17-GBS in a simplified model of CHO**
874 **cells.** (A and B) CHO, CHO- $\alpha 5\beta 1$, CHO- $\alpha v\beta 3$, CHO-ICAM1 were infected with GBS strains for 1
875 h then subjected to (A, B and E) immunofluorescence analysis or (C, D and F) CFU counts. (A)
876 Representative micrographs of untransfected or transfected CHO cells infected with CC17-GFP
877 (green). Nuclei were labeled with DAPI (blue) and actin with phalloidin (grey). Scale bar: 10 μ m.
878 (B) Representative micrographs of transfected CHO- $\alpha 5\beta 1$ infected with CC17-GFP strain (green)
879 and immunostained with anti $\alpha 5$ -integrin antibody (red). Two independent fields from the same
880 experiment are shown. Scale bar: 10 μ m. (C) Adhesion of a CC17 or a non-CC17 (CC23) strain
881 on transfected or untransfected CHO cells was quantified. Results are expressed as the % of
882 adhesion obtained on transfected cells minus that obtained on untransfected cells. (D) Adhesion
883 level of WT CC17 and derived strains on CHO- $\alpha 5\beta 1$ normalized to WT CC17 adhesion. Anti-Srr2
884 antibody was diluted 1/500. (E) CC17-GFP strain (green) was used to infect CHO- $\alpha 5\beta 1$.
885 Differential staining was realized to discriminate extracellular from intracellular bacteria. GBS
886 outside of host cells have green (GFP) and red fluorescence (anti-GBS) and appear yellow/red,
887 whereas bacteria inside host cells have green fluorescence only. Nuclei were labeled with DAPI
888 (blue) and actin was stained using phalloidin (grey). Scale bar: 10 μ m. Boxed area corresponds
889 to magnification of inset. (F) Invasion of CC17 strain or $\Delta srr2$ -derived strain on untransfected CHO
890 or CHO- $\alpha 5\beta 1$ was quantified by CFU counts. All experiments were performed at least three times
891 with each condition.

892 Statistical analysis: Data shown are mean \pm SEM of at least 3 independent experiments realized
893 in triplicate. One-Way ANOVA with Tukey's (C, F), Dunn's (D) multiple comparison test were
894 performed. NS, non-significant; *, $p < 0.05$; **, $p < 0.01$; *** $p < 0.001$.

895 **Figure 4: $\alpha 5\beta 1$ and $\alpha v\beta 3$ integrins promote Srr2 dependent CC17-GBS attachment and**
896 **invasion of cerebral endothelial cells.** (A, B) Adhesion of GBS strains onto hCMEC/D3 was
897 assessed by CFU counts (A) at MOI 10 (B) at MOI 1 in the absence or the presence of 10 $\mu\text{g/ml}$
898 of recombinant human soluble $\alpha 5\beta 1$ (s- $\alpha 5\beta 1$ integrin) or $\alpha v\beta 3$ (s- $\alpha v\beta 3$ integrin) or a mix of both
899 integrins (s- $\alpha 5\beta 1$ + s- $\alpha v\beta 3$ integrins), or ICAM1 (s-ICAM1). For each strain, results were
900 normalized to those obtained in the control experiment (untreated). (C, D) Depletion of relevant
901 integrin subunit in siRNA knockdown of (C) $\alpha 5$ integrin (D) $\beta 3$ integrin in hCMEC/D3 were analyzed
902 by Western Blot. (E) Adhesion of GBS strains onto cerebral endothelial cells, control (si-scramble),
903 $\alpha 5$ integrin-depleted (si- $\alpha 5$ integrin), $\beta 3$ integrin-depleted (si- $\beta 3$ integrin), $\alpha 5$ and $\beta 3$ integrin-
904 depleted (si- $\alpha 5$ + si- $\beta 3$ integrins), quantified by CFU following a 1 h infection. For each strain,
905 results were normalized to those obtained in the control experiment (si-scramble). (F) CC17-GFP
906 strain (green) was used to infect cerebral endothelial cells. Differential staining allowing to
907 discriminate intracellular (green) from extracellular (green + red) bacteria was performed as in Fig.
908 3E. Nuclei: DAPI (blue) and ZO1 (grey). Scale bar: 5 μm . (G) Invasion of GBS strains in
909 hCMEC/D3 was quantified by CFU counts. (H) Invasion of GBS strains in hCMEC/D3. For each
910 strain, results were normalized to those obtained in the control experiment (si-scramble). (H)
911 Invasion of CC17 strain in hCMEC/D3 was realized in the presence of host cell signaling inhibitors
912 and normalized to untreated condition.

913 Statistical analysis: Experiments were performed at least three times with each condition in
914 triplicate and expressed as mean \pm SEM. One-Way ANOVA with Dunn's multiple comparison test
915 were performed. NS, non-significant; * $p < 0.05$; **, $p < 0.01$, ****, $p < 0.0001$.

916 **Figure 5: $\alpha 5\beta 1$ and $\alpha v\beta 3$ integrins are overexpressed during the post-natal period.**
917 Expression of $\alpha 5\beta 1$ or $\alpha v\beta 3$ integrins in neonates (Neo.) or adults (Ad.) were analyzed by (A and

918 C) immunofluorescence (N=2), (B and D) Western Blot (N=3) or (E and F) immunohistochemistry
919 (N=2). (A and B) Purified rat brain vessels (BV) were labeled with specific antibodies to (A) $\alpha 5$
920 integrin to visualize $\alpha 5\beta 1$ expression or (B) $\beta 3$ integrin to visualize $\alpha v\beta 3$ expression. BV were
921 counter-stained using FITC-isolectin B4 and nuclei were labeled with DAPI. Scale bar: 20 μm .
922 Similar contrast adjustment was applied between neonates and adults images. (C and D) 100 μg
923 of rat (C) BV or (D) choroid plexus from 4th ventricle (CP4V) or lateral ventricles (CPLV) were
924 subjected to Western Blot analysis. Actin was used as loading control. (E and F) Sections of
925 human brain tissue were subjected to immunohistochemistry using antibodies to $\alpha 5$ or $\beta 3$ integrins
926 to visualize $\alpha 5\beta 1$ or $\alpha v\beta 3$ respectively, then counterstained with hematoxylin. Representative
927 micrographs of cortex allowing to visualize (E) BV, scale bar: 100 μm or (F) choroid plexuses,
928 scale bar: 50 μm . Arrows indicate BV from choroid vessels displaying positive staining; arrow-
929 heads indicate BV displaying negative staining. Boxed areas correspond to magnification of insets.

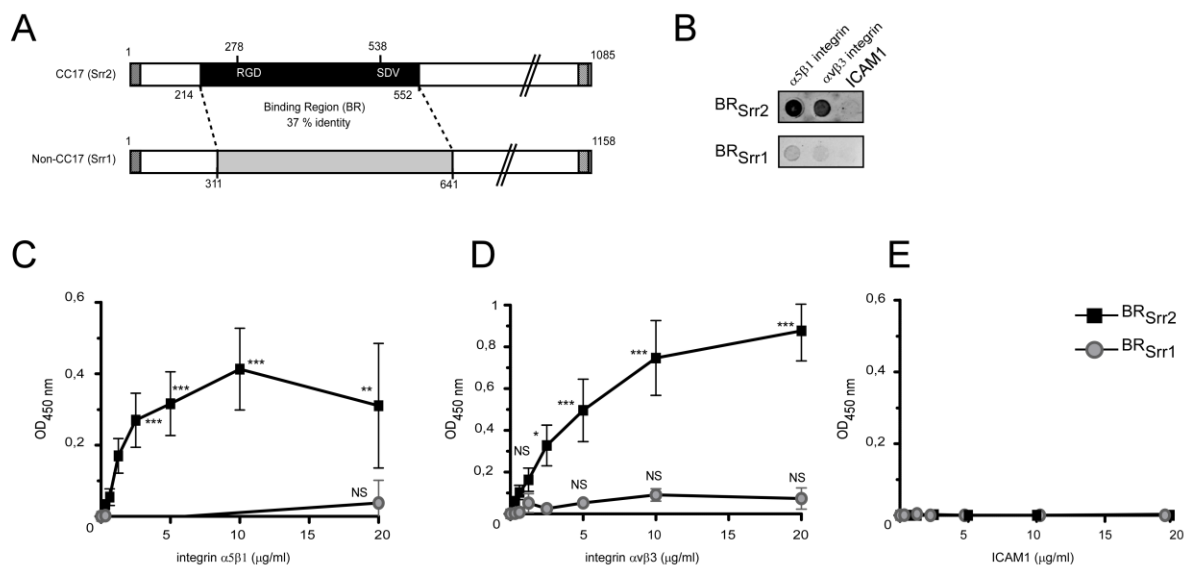
930 **Figure 6: Initial brain penetration of CC17-GBS occurs via blood vessels from the cortex**
931 **and the choroid plexuses.** Expression of $\alpha 5\beta 1$ or $\alpha v\beta 3$ integrins on purified brain vessels (BV)
932 from neonatal (Neo.), juvenile (Juv.) or adult (Ad.) Balb/C mice was analyzed by Western Blot
933 (N=2) (A) Juvenile mice were infected for 4 h with CC17-GFP strain (green) (N=2). Cerebral blood
934 vessels were stained with CD31 (red) and choroid plexus with anti-TTR (cyan). Cortex (B) and
935 choroid plexuses from the lateral ventricles (C) were examined. CC17-GFP bacteria were found
936 associated with blood vessels (arrowheads) and at distance from blood vessels (arrows). Scale
937 bar = 5 μm .

938 **Figure 7: $\alpha 5\beta 1$ and $\alpha v\beta 3$ integrins contribute to the juvenile-specific CC17-GBS-elicited**
939 **meningitis *in vivo*.**

940 Juvenile or adult Balb/C mice were infected by intravenous injection with WT CC17 (white circles)
941 or $\Delta srr2$ mutant (black squares) for 4h. Mice were euthanized and bacterial loads in blood
942 (CFU/ml) (A) and brain (CFU/g) (B) were quantified. Each symbol represents the numeration from

943 one organ from one mouse. Red horizontal lines indicate medians. Statistical analysis: Two-Way
944 ANOVA with Bonferroni's post-test was performed. NS, non-significant; * $p < 0.05$; **, $p < 0.01$.
945 Juvenile Balb/C mice were pre-treated by (C and D) intravenous injection of 10 μg of anti- $\alpha 5$
946 antibody to block $\alpha 5\beta 1$ integrin or 10 μg of isotype control, or (E and F) 5 mg/kg of RGDfV mimetic
947 peptide to block $\alpha v\beta 3$ or control vehicle (PBS). One hour after pre-treatment, mice were infected
948 by intravenous injection with 2×10^7 CFU of WT CC17 (C and E) or $\Delta srr2$ mutant (D and F) for 4 h.
949 Mice were euthanized and bacterial loads in blood (CFU/ml), spleen, liver, and brain (CFU/g) were
950 quantified. Each symbol represents the numeration from one organ from one mouse. White circles:
951 control mice; black squares: treated mice. Red horizontal lines indicate medians. Statistical
952 analysis: Mann-Whitney t test were performed with, NS, non-significant; *, $p < 0.05$; **, $p < 0.01$.
953

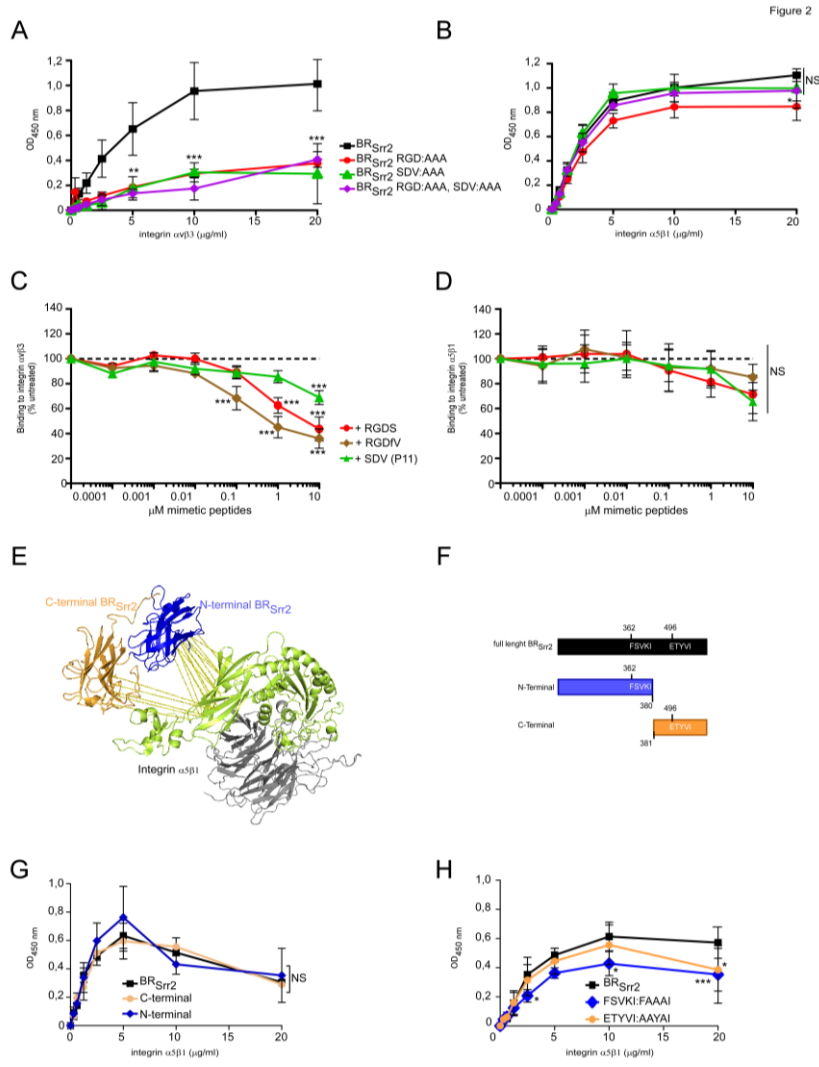
Figure 1



954
 955 **Figure 1: BR_{Srr2} recognizes α5β1 and αvβ3 integrins in a direct manner.** (A) Schematic
 956 representation of Srr2 and Srr1 proteins with signal sequence (checked), serine-rich regions
 957 (white), LPxTG cell wall anchoring motif (hatched) and the binding regions of Srr2 (black) or Srr1
 958 (grey) delineated by dashed lines. Numbers in black indicate the position of amino acid residues
 959 and letters in white indicate the predicted motifs of interaction with integrins. (B) Dot Blotting was
 960 performed to determine the interaction between immobilized human α5β1, αvβ3 integrins or
 961 ICAM1 and BR_{Srr2} or BR_{Srr1}. Purified BR_{Srr2} and BR_{Srr1} proteins are shown in Fig. S1A. (C, D and
 962 E) Interaction of BR_{Srr2} (black squares) or BR_{Srr1} (grey circles) with human α5β1 integrin (C), αvβ3
 963 integrin (D) or ICAM1 (E) were assessed by ELISA. Results were normalized to negative control
 964 (BSA). Statistical analysis: data shown are mean ± SEM of at least three independent
 965 experiments. Two-Way ANOVA with Bonferroni's multiple comparisons post-test was performed.
 966 NS, non-significant; *, $p < 0.05$; **, $p < 0.01$; ***, $p < 0.001$.

967

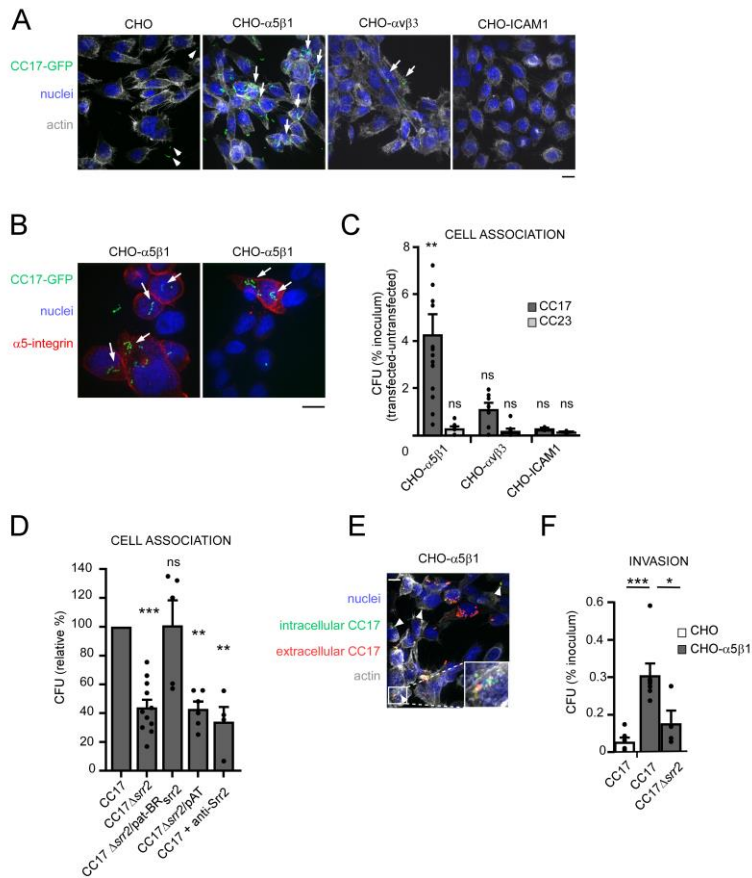
968



969

970 **Figure 2: Identification of BR_{Srr2} residues involved in the direct interaction with $\alpha\beta3$ and**
 971 **$\alpha5\beta1$ integrins.** (A and B) Interaction of BR_{Srr2}, or its mutated forms, with integrins $\alpha\beta3$ (A) or
 972 $\alpha5\beta1$ (B) were assessed by ELISA. Mutated forms of BR_{Srr2} proteins are shown in Supplementary
 973 Fig. S1B and C. (C and D) Interaction of BR_{Srr2} with integrins $\alpha\beta3$ (C) or $\alpha5\beta1$ (D) in the presence
 974 of increasing concentration of mimetic peptides were assessed by ELISA. Results were expressed
 975 as % of untreated condition. (E) Graphic representation of predicted contacts between BR_{Srr2} and
 976 $\alpha5\beta1$ integrin identified by RaptorX (Fig. S4). RaptorX mapped on the $\alpha5$ (grey) $\beta1$ (green) integrin
 977 subunits predicted two contact zones located in the N-terminal (blue) and C-terminal (gold)
 978 domains of BR_{Srr2}. Only the most reliable contacts (contact probability >0.7) are depicted as yellow
 979 lines in the scheme. (F) Schematic representation of BR_{Srr2} or its truncated forms. Numbers in
 980 black indicate the position of amino acid residues in Srr2, and letters in white the predicted motifs
 981 of interaction with the integrin $\alpha5\beta1$. (G) ELISA assays with integrin $\alpha5\beta1$ were performed using
 982 equimolar amounts of coated BR_{Srr2} or of its truncated forms. (H) Interaction of BR_{Srr2}, or its
 983 mutated forms, with the integrin $\alpha5\beta1$ were assessed by ELISA. Mutated forms of BR_{Srr2} proteins
 984 are shown in Fig. S1D and E.

985 ELISA results were normalized to the negative control (BSA). Statistical analysis: data shown are
 986 mean \pm SEM of at least three independent experiments. Two-Way ANOVA with Bonferroni's
 987 multiple comparisons post-test was performed. NS, non-significant; *, $p < 0.05$; **, $p < 0.01$; ***, p
 988 < 0.001 .

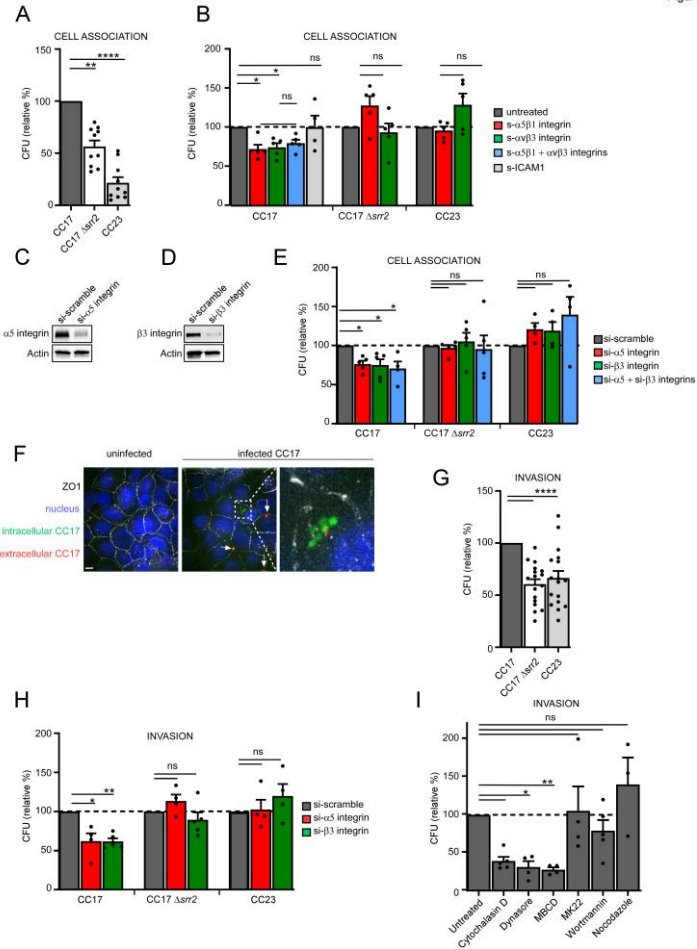


989

990 **Figure 3: $\alpha 5\beta 1$ promotes adhesion and invasion of CC17-GBS in a simplified model of CHO**
 991 **cells.** (A and B) CHO, CHO- $\alpha 5\beta 1$, CHO- $\alpha v\beta 3$, CHO-ICAM1 were infected with GBS strains for 1
 992 h then subjected to (A, B and E) immunofluorescence analysis or (C, D and F) CFU counts. (A)
 993 Representative micrographs of untransfected or transfected CHO cells infected with CC17-GFP
 994 (green). Nuclei were labeled with DAPI (blue) and actin with phalloidin (grey). Scale bar: 10 μ m.
 995 (B) Representative micrographs of transfected CHO- $\alpha 5\beta 1$ infected with CC17-GFP strain (green)
 996 and immunostained with anti $\alpha 5$ -integrin antibody (red). Two independent fields from the same
 997 experiment are shown. Scale bar: 10 μ m. (C) Adhesion of a CC17 or a non-CC17 (CC23) strain
 998 on transfected or untransfected CHO cells was quantified. Results are expressed as the % of
 999 adhesion obtained on transfected cells minus that obtained on untransfected cells. (D) Adhesion
 1000 level of WT CC17 and derived strains on CHO- $\alpha 5\beta 1$ normalized to WT CC17 adhesion. Anti-Srr2
 1001 antibody was diluted 1/500. (E) CC17-GFP strain (green) was used to infect CHO- $\alpha 5\beta 1$.
 1002 Differential staining was realized to discriminate extracellular from intracellular bacteria. GBS
 1003 outside of host cells have green (GFP) and red fluorescence (anti-GBS) and appear yellow/red,
 1004 whereas bacteria inside host cells have green fluorescence only. Nuclei were labeled with DAPI
 1005 (blue) and actin was stained using phalloidin (grey). Scale bar: 10 μ m. Boxed area corresponds
 1006 to magnification of inset. (F) Invasion of CC17 strain or $\Delta srr2$ -derived strain on untransfected CHO
 1007 or CHO- $\alpha 5\beta 1$ was quantified by CFU counts.

1008 Statistical analysis: Data shown are mean \pm SEM of at least 3 independent experiments realized
 1009 in triplicate. One-Way ANOVA with Tukey's (C, F), Dunn's (D) multiple comparison test were
 1010 performed. NS, non-significant; *, $p < 0.05$; **, $p < 0.01$; *** $p < 0.001$. All experiments were
 1011 performed at least three times with each condition.

Figure 4



1012

1013 **Figure 4: $\alpha 5\beta 1$ and $\alpha v\beta 3$ integrins promote *Srr2* dependent CC17-GBS attachment and**
 1014 **invasion of cerebral endothelial cells.** (A, B) Adhesion of GBS strains onto hCMEC/D3 was
 1015 assessed by CFU counts (A) at MOI 10 (B) at MOI 1 in the absence or the presence of 10 $\mu\text{g/ml}$
 1016 of recombinant human soluble $\alpha 5\beta 1$ (s- $\alpha 5\beta 1$ integrin) or $\alpha v\beta 3$ (s- $\alpha v\beta 3$ integrin) or a mix of both
 1017 integrins (s- $\alpha 5\beta 1$ + s- $\alpha v\beta 3$ integrins), or ICAM1 (s-ICAM1). For each strain, results were
 1018 normalized to those obtained in the control experiment (untreated). (C, D) Depletion of relevant
 1019 integrin subunit in siRNA knockdown of (C) $\alpha 5$ integrin (D) $\beta 3$ integrin in hCMEC/D3 were analyzed
 1020 by Western Blot. (E) Adhesion of GBS strains onto cerebral endothelial cells, control (si-scramble),
 1021 $\alpha 5$ integrin-depleted (si- $\alpha 5$ integrin), $\beta 3$ integrin-depleted (si- $\beta 3$ integrin), $\alpha 5$ and $\beta 3$ integrin-
 1022 depleted (si- $\alpha 5$ + si- $\beta 3$ integrins), quantified by CFU following a 1 h infection. For each strain,
 1023 results were normalized to those obtained in the control experiment (si-scramble). (F) CC17-GFP
 1024 strain (green) was used to infect cerebral endothelial cells. Differential staining allowing to
 1025 discriminate intracellular (green) from extracellular (green + red) bacteria was performed as in Fig.
 1026 3E. Nuclei: DAPI (blue) and ZO1 (grey). Scale bar: 5 μm . (G) Invasion of GBS strains in
 1027 hCMEC/D3 was quantified by CFU counts. (H) Invasion of GBS strains in hCMEC/D3. For each
 1028 strain, results were normalized to those obtained in the control experiment (si-scramble). (H)
 1029 Invasion of CC17 strain in hCMEC/D3 was realized in the presence of host cell signaling inhibitors
 1030 and normalized to untreated condition.
 1031 Statistical analysis: Experiments were performed at least three times with each condition in
 1032 triplicate and expressed as mean \pm SEM. One-Way ANOVA with Dunn's multiple comparison test
 1033 were performed. NS, non-significant; * $p < 0.05$; ** $p < 0.01$, ****, $p < 0.0001$.

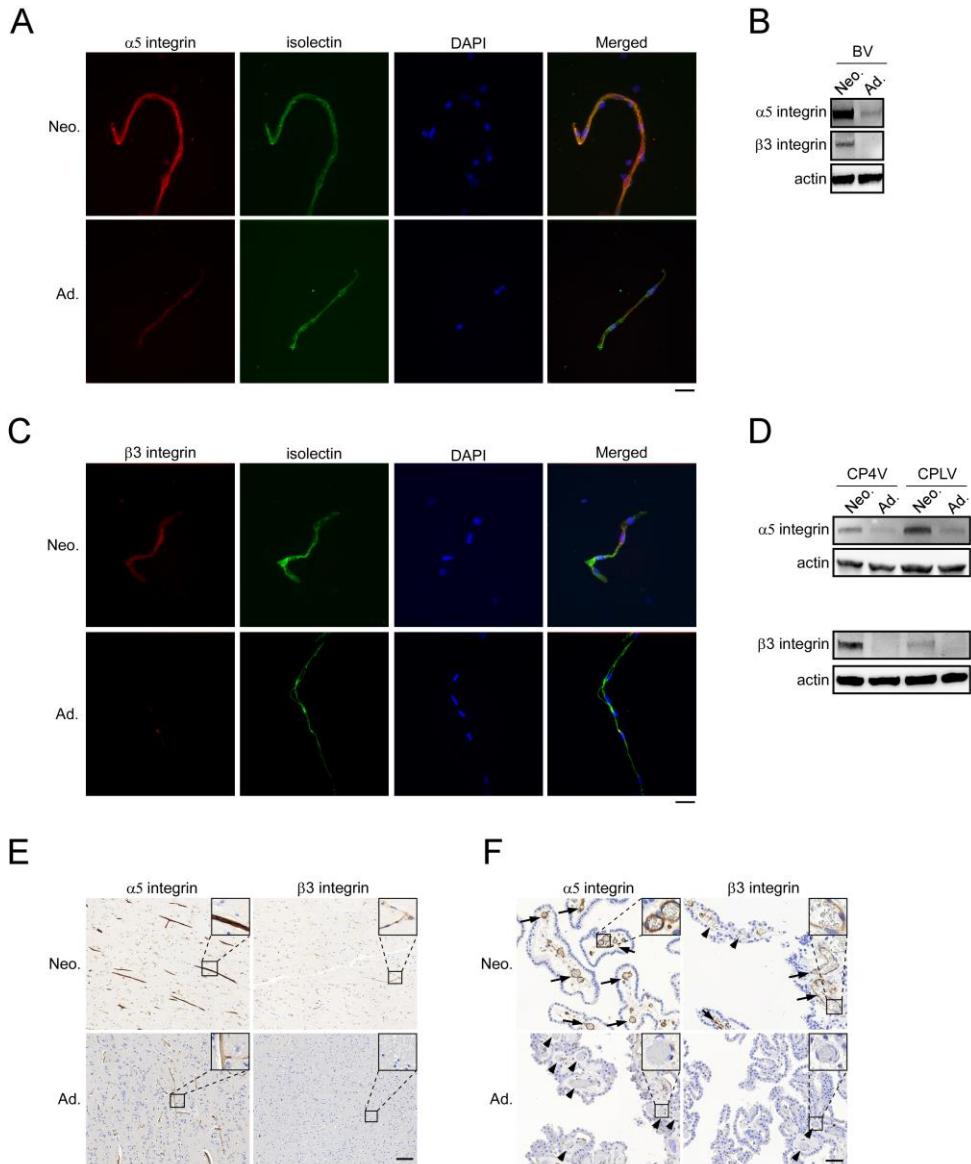
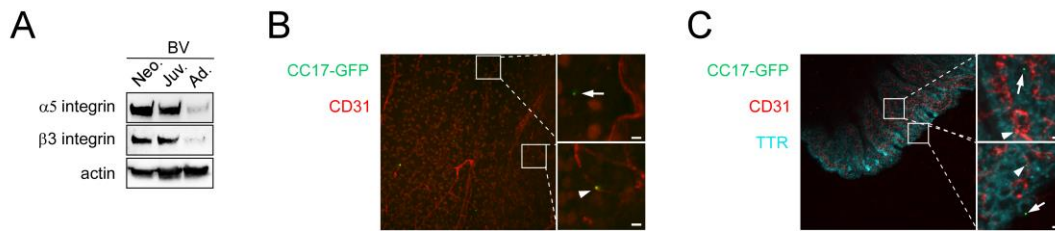


Figure 5

1034

1035 **Figure 5: $\alpha 5\beta 1$ and $\alpha v\beta 3$ integrins are overexpressed during the post-natal period.**
 1036 Expression of $\alpha 5\beta 1$ or $\alpha v\beta 3$ integrins in neonates (Neo.) or adults (Ad.) were analyzed by (A and
 1037 C) immunofluorescence (N=2), (B and D) Western Blot (N=3) or (E and F) immunohistochemistry
 1038 (N=2). (A and B) Purified rat brain vessels (BV) were labeled with specific antibodies to (A) $\alpha 5$
 1039 integrin to visualize $\alpha 5\beta 1$ expression or (B) $\beta 3$ integrin to visualize $\alpha v\beta 3$ expression. BV were
 1040 counter-stained using FITC-isolectin B4 and nuclei were labeled with DAPI. Scale bar: 20 μ m.
 1041 Similar contrast adjustment was applied between neonates and adults images. (C and D) 100 μ g
 1042 of rat (C) BV or (D) choroid plexus from 4th ventricle (CP4V) or lateral ventricles (CPLV) were
 1043 subjected to Western Blot analysis. Actin was used as loading control. (E and F) Sections of
 1044 human brain tissue were subjected to immunohistochemistry using antibodies to $\alpha 5$ or $\beta 3$ integrins
 1045 to visualize $\alpha 5\beta 1$ or $\alpha v\beta 3$ respectively, then counterstained with hematoxylin. Representative
 1046 micrographs of cortex allowing to visualize (E) BV, scale bar: 100 μ m or (F) choroid plexuses,
 1047 scale bar: 50 μ m. Arrows indicate BV from choroid vessels displaying positive staining; arrow-
 1048 heads indicate BV displaying negative staining. Boxed areas correspond to magnification of insets.



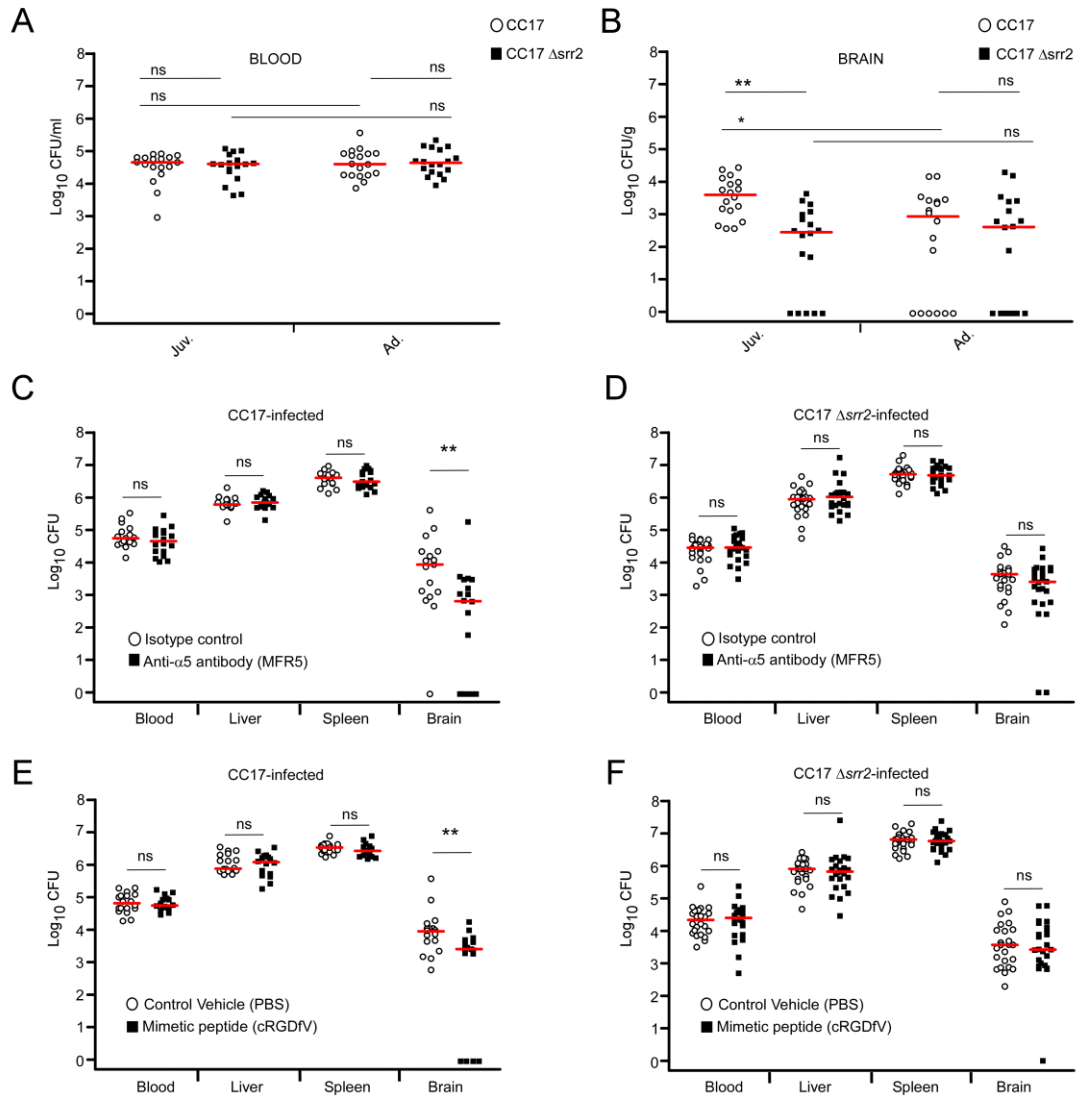
1049

1050 **Figure 6: Initial brain penetration of CC17-GBS occurs *via* blood vessels from the cortex**
 1051 **and the choroid plexuses.** Expression of $\alpha 5\beta 1$ or $\alpha \nu\beta 3$ integrins on purified brain vessels (BV)
 1052 from neonatal (Neo.), juvenile (Juv.) or adult (Ad.) Balb/C mice was analyzed by Western Blot
 1053 (N=2) (A) Juvenile mice were infected for 4 h with CC17-GFP strain (green) (N=2). Cerebral blood
 1054 vessels were stained with CD31 (red) and choroid plexus with anti-TTR (cyan). Cortex (B) and
 1055 choroid plexuses from the lateral ventricles (C) were examined. CC17-GFP bacteria were found
 1056 associated with blood vessels (arrowheads) and at distance from blood vessels (arrows). Scale
 1057 bar = 5 μm .

1058

1059

Figure 7



1060

1061 **Figure 7: α 5 β 1 and α v β 3 integrins contribute to the juvenile-specific CC17-GBS-elicited**
 1062 **meningitis *in vivo*.** Juvenile or adult Balb/C mice were infected by intravenous injection with WT
 1063 CC17 (white circles) or Δ srr2 mutant (black squares) for 4h. Mice were euthanized and bacterial
 1064 loads in blood (CFU/ml) (A) and brain (CFU/g) (B) were quantified. Each symbol represents the
 1065 numeration from one organ from one mouse. Red horizontal lines indicate medians. Statistical
 1066 analysis: Two-Way ANOVA with Bonferroni's post-test was performed. NS, non-significant; * p <
 1067 0.05; **, p < 0.01.

1068 Juvenile Balb/C mice were pre-treated by (C and D) intravenous injection of 10 μ g of anti- α 5
 1069 antibody to block α 5 β 1 integrin or 10 μ g of isotype control, or (E and F) 5 mg/kg of RGDFV
 1070 mimetic peptide to block α v β 3 or control vehicle (PBS). One hour after pre-treatment, mice were
 1071 infected by intravenous injection with 2×10^7 CFU of WT CC17 (C and E) or Δ srr2 mutant (D and F)
 1072 for 4 h. Mice were euthanized and bacterial loads in blood (CFU/ml), spleen, liver, and brain (CFU/g)
 1073 were quantified. Each symbol represents the numeration from one organ from one mouse. White
 1074 circles: control mice; black squares: treated mice. Red horizontal lines indicate medians. Statistical
 1075 analysis: Mann-Whitney t test were performed with, NS, non-significant; *, p < 0.05; **, p < 0.01.